SCHOOL OF ELECTRICAL ENGINEERING AND TELECOMMUNICATIONS

Resource Allocation and Beamforming Design for Max-min Fair IRS-assisted Networks

by

Yimin Xu

Thesis submitted as a requirement for the degree of

Master of Engineering (Electrical Engineering)

Submitted: Aug. 27, 2022

Abstract

Massive multiple-input multiple-output (M-MIMO), millimeter-wave (mmWave), and ultra-densification are the core technologies used in the fifth-generation (5G) communication systems. Although their utilization remarkably enhances the system performance, they also pose many challenges, including the huge energy consumption of M-MIMO, the limited transmission coverage of mmWave, as well as both resource congestion and charging problems associated with ultra-densification. As a result, it is imperative to adopt novel technologies to mitigate these problems.

Accordingly, this dissertation develops resource allocation algorithms based on an IRS-aided SWIPT sensor network, while guaranteeing the fairness of the individual data rate. Since the proposed system employs a linear energy harvesting (EH) model, the beamforming vectors at the base station (BS), the phase shifts at the IRS, as well as power splitting (PS) are jointly optimized to maximize the minimum value of individual achievable data rate.

The original problem formulation is non-convex due to the multiplication of optimization variables. By using the alternating optimization (AO) algorithm, it can be decomposed into two subproblems. Accordingly, two algorithms, namely semidefinite programming relaxation (SDR)-based successive convex approximation (SCA) and penalty-based SCA, are used to handle these two subproblems with rank-one constraint, respectively. In the simulation results, we confirm the effectiveness of IRS for SWIPT-MISO communication system.

Keywords— intelligent reflecting surface (IRS), simultaneous wireless information and power transfer (SWIPT), max-min fairness, SCA.

Acknowledgements

I would like to express my sincere gratitude to my supervisor Derrick Wing Kwan Ng, who guided me throughout this project. Without Derrick's support and guidance, I cannot find that academics can be so charming. Throughout my life, I will cherish this experience and be forever grateful for all meaningful stories shared by my professor which helped me rethink the direction of my future. I also wish to thank my parents and my friends Rena and Bruce for supporting me through difficult time and giving me courage and confidence.

Abbreviations

5G Fifth-generation

AO Alternating Optimization

AS Antenna Switching

AWGN Addictive White Gaussian Noise

BS Base Station

CDMA Code-division Multiple Access

DoF Degrees-of-Freedom

EDGE Enhanced Data rates for GSM Evolution

EH Energy Harvesting

EVD Eigenvalue Decomposition

GSM Global System for Mobile Communications

HD High Definition

ID Information Decoding

IOS Intelligent Omni-Surface

IRS Intelligent Reflecting Surface

LTE Long Term Evolution

LoS Line-of-Sight

M-MIMO Massive Multiple-Input Multiple-Output

mmWave Millimeter-wave

OFDM Orthogonal Frequency-Division Multiplexing

PS Power Splitting

QoS Quality of Service

RF Radio Frequency

SCA Successive Convex Approximation

SDP Semidefinite Programming

SDR Semidefinite Programming Relaxation

SINR Signal-to-Interference-plus-noise Ratio

SWIPT Simultaneous Wireless Information and Power Transfer

TS Time Switching

UAV Unmanned Aerial Vehicle

UHF Ultra-High-Frequency

UMTS Universal Mobile Telecommunications Service

WiMax Worldwide Interoperability for Microwave Access

WIT Wireless Information Transfer

WPBC Wireless-Powered Backscatter Communication

WPC Wireless-Powered Communication

WPT Wireless Power Transfer

Contents

List of Figures

List of Tables

Chapter 1

Introduction

To target the updating communication standards, we has witnessed tremendous growth in the wireless industry with mature protocols, wider-spectrum, and even reconfigurable channel being designed [3]. Thereby, the last few decades have experienced a remarkable evolution from the first generation (1G) to 5G.

The 1G cellular networks were first introduced in 1981, which only provided voice service with 2 Kbps data rate by the cordless communication system [4]. To improve the poor data service, the concept of the second generation (2G), e.g. Global System for Mobile Communications (GSM), was proposed with objections in reduced communication fees, higher data rate (up to 64 Kbps), and extra text messaging service [5]. With the development of smartphone, the third generation (3G) networks gradually replaced the 2G system, where 3G networks depend on more mature concepts, such as code-division multiple access (CDMA), Universal Mobile Telecommunications Service (UMTS), Enhanced Data rates for GSM Evolution (EDGE), and so on. The 3G networks are able to support video conference, mobile TV, and even wireless mobile Internet with high speed (approximate up to 2 Mbps) [6]. However, since 3G systems provide limited bandwidth resources, then the need for spectrum improvement gave birth to the fourth generation(4G). The 4G networks, e.g. Long Term Evolution (LTE) and Worldwide Interoperability for Microwave Access (WiMax), are able to offer up to 1 Gbps data speed which enables video communication and High Definition (HD) moving sharing [7]-[10]. When the number of electric devices and mobile subscribers keeps a growing trend, the intense demands for better services and additional spectrum push the 4G networks to evolve into advanced fifth-generation (5G) systems with extremely high rates, e.g.

at least 1 Gbps, low latency, e.g. as low as the order of 1-millisecond, and extended capacity [11, 12]. Due to the outstanding transmission performance in 5G networks, point-to-point communication in 1G to 4G would gradually move to network-to-network communication, which enables self-driving car, remotes surgery in healthcare, and even machine-to-machine communication in the near future [13, 14]. Indeed, a lots of advanced techniques, such as ultra-densification, mmWave,small cells, and M-MIMO, contribute to the implementation of 5G or even beyond 5G networks [15]. A simple comparison of 1G to 5G system are summarized in Table 1.1. Although those 5G-related techniques

Table 1.1: Comparison of 1G, 2G, 3G, 4G, 5G Cellular Systems

	1G	2G	3G	4G	5G
Key Ref.	[3],[4]	[5],[6]	[5],[6]	[7],[9],[10]	[11],[12],[14]
Capacity	2 Kbps	14.4-64 Kbps	144 Kbps-2 Mpbs	100 Mbps-1 Gbps	1 Gbps and higher
Bandwidth	150/900 MHz	900 MHz	100 MHz	100 MHz	1000xBW per unit area
Frequency	30 KHz	1.8 GHz	1.6-2.0 GHz	2.0-8.0 GHz	3-300 GHz
Main Technologies	Analog Cellular	Digital Cellular	CDMA,UMTS,EDG	Wide-area Network	Ultra-densification, mmWave, Massive MIMO
Main Objections	Voice service	Short messages	Video conferencing, Mobile TV	Mobile Multimedia	Machine-to-machine communication, Remote control of vehicles, Medical procedures

provide considerable improvement in system performance, they lead to some side effects in commercial deployment of 5G networks, for example, huge facilities cost, higher power consumption, or fading. It is imperative to find some solutions to alleviate those issues and construct sustainable future wireless networks with energy and spectral efficiency [16].

In light of this, we first introduce the major challenges emerging in 5G systems in Section 1.1. In Section 1.2, we briefly review the technology of IRS and the corresponding model, respectively. In Section 1.3, we elaborate on two common fairness protocols, i.e. proportional fairness and max-min fairness. In Section 1.4, we provide the basic concept of power transfer. In Section 1.5, we elaborate some prior related works. The thesis organization is provided in Section 1.6.

1.1 Overview of 5G networks Challenges and Technologies

Although new technologies such as mmWave and mMIMO improve energy and spectrum efficiency and throughput, they also introduce new unprecedented challenges which make the blueprint of the commercializing 5G systems impossible in the future. Thereby,the possible and promising solutions for those challenges are envisaged in Figure 1.1.

technology,challenge, solution.pdf

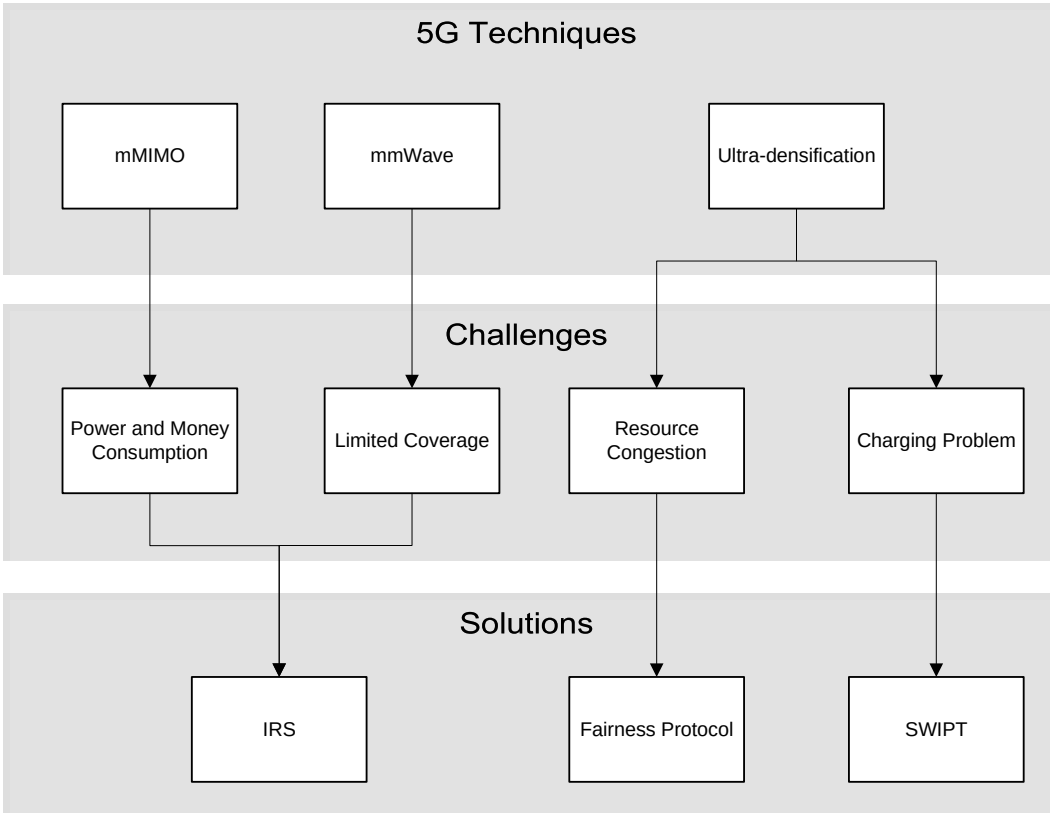

Figure 1.1: Diagram for major techniques, challenges and related solutions in 5G networks.

1.2 IRS Technology

1.2.1 Massive MIMO-Related Challenges

To exploit potential multiplexing and diversity gain with enhanced spectral efficiency, 5G communication deploy an unprecedented number of antennas in both transmitter side and

receiver side. The massive MIMO technique, on the one hand, increases system throughput, offers favorable propagation conditions by the orthogonal property and enhances the capacity through mitigating the inter-user interference [11]. However, those performance enhancements come at the expense of more expensive hardware, more energy use, and more sophisticated signal processing. The cost-effective demand enables new materials to replace some antennas in the massive MIMO systems. As such, IRS with passive elements can be promising leveraged to reduce some parts of active antenna in massive MIMO yielding into hybrid networks,as a result of cost reduction, flexible deployment, and energy conservation [17].

1.2.2 mmWave-Related Challenges

In 5G networks, the mmWave technology has stood out as an enabler to satisfy the explosive data rate requirements by exploiting unused and unlicensed spectrum to carry information leading to data rates up to gigabits per second [11]. However, the extremely high frequency of mmWave bands does not come for free which results in an intractable coverage problem. For example, the frequency of mmWave can occupy in $1-30$ GHz with the corresponding extremely short wavelength in the range of $1-10$ mm [18]. The shorter wavelength leads to poor ability in diffraction, scattering, and high atmospheric attenuation loss caused by fog or rain. To ensure the quality of mmWave communication where the signal power is strong enough to be detected at receiver, the required line-of-sight (LOS) path or reducing the transmission range is essential in system design [13]. Therefore, IRSs have received considerable attention in terms of their ability to reconfigure the channel condition and provide a virtual LoS link to ultra-high-frequency (UHF) signals.

1.2.3 Basic Concept of IRS

Accordingly, there are two remarkable bottlenecks in 5G system, including limited coverage problem due to penetration loss in mmWave frequencies and high hardware cost due to increasing multiple antenna deployment in massive MIMO. Those challenges are major force to promote the development of the IRS-empowered system, since IRS is capable of providing many undeniable advantages, for example, extending the limited coverage, nulling interference to zero, and low energy consumption.

It is worth noting that IRS has a relatively simple manufacturing process whose architecture looks like a two-dimensional sandwich [19]. Specifically, IRS is a piece of an artificial thin surface with three layers that contain some reflecting meta-atom, copper backplane, control circuit board, and a smart controller [20]. The smart controller can operate each passive reflecting element to adjust the phase, amplitude, or polarization of the incident signal. This is controlled to leverage the reflecting signal in a well-designed direction. Thereby, an uncontrollable random radio environment becomes programmable and deterministic [21]. In addition, IRS can also use the on-off states of reflecting elements to transmit extra information, as studied in the [22] and [23].

Application1.pdf

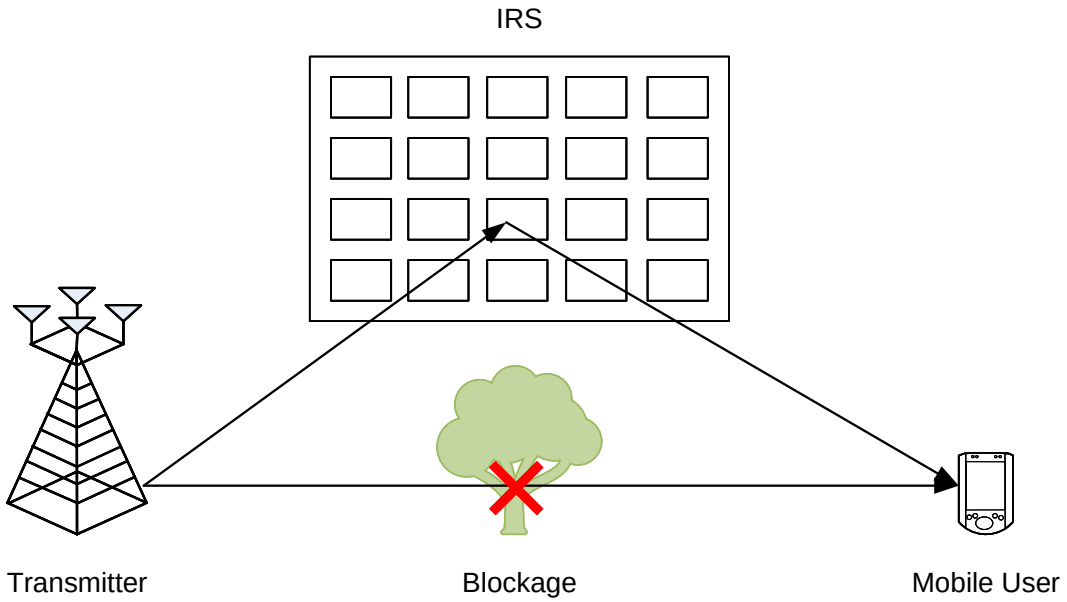

Figure 1.2: The directed link was blocked by a tree and an IRS is deployed to establish a new link for transmitter and mobile receiver.

Based on its special material and passive properties, IRSs can offer plenty of advantages over traditional equipment such as relays or backscatters. Firstly, as a prominent feature, IRS is envisioned to offer coverage extension for mmWave communication, where IRS can help radio frequency (RF) signal bypass blockage via passive reflection. Based on this property, engineers are capable to tailor the propagation path in the wireless network [17]. Furthermore, IRS is a promising candidate for an economical and energy-efficient wireless system. Because IRS can operate in the absence of RF chains, as such, its scatter elements usually consume at most 1 mW [19]. The new hybrid wireless communication

system comprising both active antennas and passive IRS leverages scalable consumption and energy efficiency [24]. Thirdly, different from the unwieldy active nodes, IRS can be flexibly deployed in practical implementation due to its lightweight and low profile [25]. This feature is greatly useful enabling the future densely deployment of IRS seamless integration into windows, ceilings, or building facades. In light of many benefits of

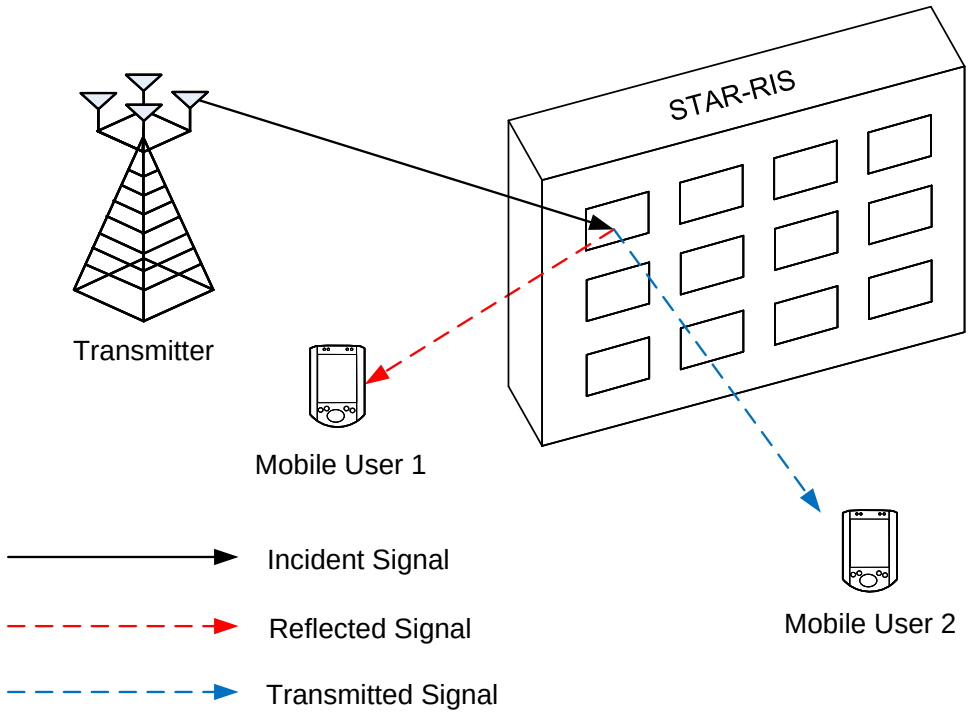

Figure 1.3: With the help of STAR-RIS, the transmitter can simultaneously send signals to individual mobile users, where these users are located in both sides of the STAR-RIS.

IRS, various promising IRS-aided network scenarios with different objections have been studied. For example, a popular use case of IRS-aided system is related to the blockage channel, cf. Figure 1.2, where IRS customizes a virtual line-of-sight (LoS) link to circumvent the obstacles existing in the propagation path [20]. This application is appealing to overcome the challenge of coverage limitations in mmWave communications. In addition to achieving a virtual LoS path, some studies consider its application to achieve full-dimensional coverage. The initial model is simultaneously transmitting and reflecting reconfigurable intelligent surfaces (STAR-RISs) where it enables signal reflection and transmission at the same time. In Figure 1.3, it demonstrates one example of STAR-RIS aided communication where the transmitter facilitates simultaneous multiuser transmission with extended space diversity. In indoor situations or the receiver is located on

the backside of IRS, intelligent omni-surface (IOS) can further provide full-space coverage service (i.e. 360-degree coverage) by reflecting and refracting the transmitted signal [26]. Moreover, IRS is widely used to assist SWIPT systems or unmanned aerial vehicle (UAV) communication systems [27] since negative smart reflections of IRS facilitate the reduction of system power consumption and provide performance gains.

1.3 Fairness Protocol

1.3.1 Ultra-densification-Related Challenges

Another core technology used in 5G network is ultra-densification, where plenty of intelligent devices with wireless connectively provide high capacity demand, support diverse mobility environments, and better performance gain [28]. However, ultra-densification incurs concerns about resource allocation, as billions of devices compete for the same resources, such as power, spectrum, or space. The baseline for resource allocation is to ensure minimum QoS requirements and individual service and avoid resource famine even with exhausting the system resource [29]. At the same time, ultra-densification is the major culprit in resource congestion, energy redundancy, or even spectral waste without efficient fair resource allocation [30]. Therefore, fairness consideration is indispensable for the current implementation of ultra-dense networks with reliable QoS services.

1.3.2 Fairness Resource Allocation Protocol

In fact, fairness could be defined from various aspects and easily be influenced by different research areas. For example, some papers focus on fairness in a specific short time duration while some consider dynamically fairness over the time moving window [31]. Accordingly, it is impossible to provide a single authoritative definition for a rather subjective norm and a unified agreement on its definition has not been reached. So far, the well-adopted way to specify fairness is through Jain's index or entropy measure, where its value can quantify the level of fairness [32]. This index is a promising enabler to evaluate the level of fairness under different fairness criteria.

However, legacy power allocation criteria such as equal allocation or the water-filling approach suffer a poor level of fairness [33]. Take video resources as an example, users

deserve to enjoy equal video quality even under the competing streams while terrible video quality with high and frequent traffic happens to some users in the absence of a proper resource allocation scheme. In this way, the α-fairness protocol is commonly used to provide scalable criteria for fair resource allocation, where several allocation cases can be reached in the same universal framework by tweaking the parameter α [31]. Two representative allocation schemes based on α-fairness are illustrated as follows:

1) **Max-min fairness:** It is related to the extreme case of α-fairness with $\alpha = \infty$. The principle of max-min fairness introduces a guideline that the possible resources are given priority to the most poorly treated users (i.e., users with the minimum bit rates) [34].

2) **Proportional fairness:** The proportional fairness corresponds to the case of $\alpha = 1$ in α-fairness protocol. Its operation rule based on the logarithmic utility function to schedule each flow allocation proportionally fair to a fixed window flow [35].

Generally, the high value of α contributes to a favorable fairness level. The specific analysis for the α-fairness resource allocation was done in [31] in providing the relationship between α and Jain's index. They prove that α controls the balance between efficiency and fairness, especially for $\alpha = 0$ gives a relatively maximum efficiency level. In [36], T. Bonald et al. also prove setting enhanced α leads to a higher fairness level but decreases user efficiency. Especially, under the max-min fairness scheme, α goes to infinity with reaching the most fairness level, while most resources are almost assigned to the worst channel leading to severe inefficiency.

Consequently, the max-min protocol is appropriate to solve the congestion challenges and unreliable QoS service in denser 5G networks. This thesis would focus on the rate allocation based on the max-min protocol to balance the discrepancy and control rate congestion between receivers.

1.4 SWIPT Technology

1.4.1 Ultra-densification-Related Challenges

In the era of Internet-of-Things (IoT), the denser interconnection (i.e. ultra-densification) of various electronic equipment poses another challenge to current 5G architectures:

charging problem. On the one hand, there is an emergency for energy support for those devices with limited charging capability in denser networks[1]. On the other hand, the conventional wired recharging technology is inconvenient or even impossible for those devices that are in corners, especially for embedded sensors [13].

Consequently, the relentless growth in energy-limited devices and unsuitable wired charging method potentially cause an urgent demand for a new way to prolong their lifetime. Then, WPT has emerged as a promising solution to enable the large-scale deployment of battery-limited networks with significant flexibility features [37]. In addition, WPT, to some extent, can avoid the expenditure on wired cable installation and maintenance than legacy method.

1.4.2 Power Transfer Concept

Basically, the concept of WPT techniques refer to delivering the energy from transmitter to receiver without wires[38].The general system architectures diagram is presented in Figure 1.4. So far, the common implementation of WPT techniques can broadly be

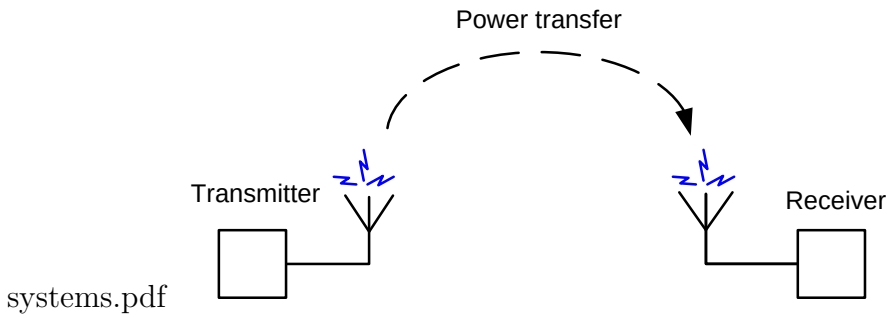

Figure 1.4: Wireless power transfer system.

categorized in two types: non-radiative (near-field) WPT and radiative (far-field) WPT [39]. Those four representative WPT technology are illustrated as follows:

1. **Inductive coupling:** The mechanism of inductive coupling WPT is based on magnetic field induction theory [40]. When the primary coil can generate a time-varying magnetic field, then the secondary coil can induce the electric current within this field. In this way, many drawbacks come along with induction coupling, including poor stability and the stringent requirement on alignment, which limits the maximum transmission distance to only several centimeters [41]. In contrast, inductive

coupling WPT can reach the highest efficiency among those methods, which is up to approximately 95% [42].

2. **Resonance coupling:** The resonance coupling WPT replies on the same resonance frequency to support power transfer and it belongs to the near-field transmission [43]. This scheme have been introduced into many portable systems such as tablets or mobile phones due to its longer coverage distance up to several meters and no tighten alignment restriction. However, the authors in [42] investigated that the resonance coupling WPT is less efficient (e.g. about 75%) compared to the resonance coupling WPT.

3. **RF-microwave power trasfer:** RF-microwave WPT refers to wireless power transfer via radio waves or microwaves, which can enable energy transmission over greater distances (e.g. up to multiple kilometers) [44]. However, the author in [45] shows that the maximum transfer efficiency of RF-microwave scheme is less than 50% without LoS path. Any obstacles would largely attenuate the transmitted microwave signal and even stop energy transmission. With the aid of high gain antennas, RF-microwave WPT can exhibit approximately 90% transmission efficiency.

4. **Laser power transfer:** The principle of laser power transfer refers that the conversion of the electric source into a high-intensity laser beam allows the energy to be transmitted to the load as a laser [46]. Considering shorter wavelength implies weaker penetrate ability, the laser beam in terahertz (THz) band would suffer from serious drawbacks of penetrating loss.

The representative properties of different types of WPT schemes are listed in Table 1.2. Although near-field WPT is equipped with additional performance merit in transfer efficiency, the distance constraints limit its practical application. In contrast, the far-field WPT with greater coverage over several kilometers is more appropriate for current denser 5G networks to supply energy and recharge batteries for mobile devices. In terms of the far-field WPT, the efficiency of microwave power beam could exceed that of laser power beam since laser power beam is more vulnerable to atmospheric blockages such as dust or rain [44]. Moreover,as a high-intensity beam, laser power transfer highly depends on line of sight or alignment to the receiver. Consequently, a proper scheme that both

satisfies long-range transmission and has better performance in environment blockages is RF-microwave power transfer in this thesis.

Table 1.2: The general classification and corresponding property of WPT technology.

	Inductive Coupling	Resonance Coupling	RF-Microwave Power Transmission	Laser Power Transmission
Key References	[40], [41], [42]	[42], [43]	[44], [45]	[46]
Sort	Non-Radiative (near-field)	Non-Radiative (near-field)	Radiative (far-field)	Radiative (far-field)
Coverage Distance	Short (cm)	Medium (m)	Long (km)	Long (km)
Operating Frequency	KHZ MHz	KHz MHz	GHz	>THz
Energy Delivery Efficiency	High	Medium	Low to Medium	Low to Medium

1.4.3 The Basic Concept of Energy Harvesting

After power transmission, the received RF signal needs to be converted into electrical energy in order to power the receiver. This type of conversion is defined as energy harvesting (EH) [47]. The combination of WPT and EH has been regarded as a key enables of green eco 5G communication, due to the ability to power the denser 5G communication devices from ambient RF signals [16].

So far, plenty of research has been proposed to optimize the practical RF energy harvesting circuit, where common circuit architecture contains a receiver antenna, a matching network or passive bandpass filter, a rectifying circuit, and the energy storage unit [1], cf. Figure 1.5. According to their circuit charging characteristic, RF-based EH model can be of two types: linear EH model and non-linear model, which are illustrated as following:

1. **Linear EH model:** This model assumes the output energy is linearly proportional to input energy [37]. Although this model is not accurate, especially for large input power, it enables a simple resource allocation design. As a result, many early

Harvesting Model.pdf

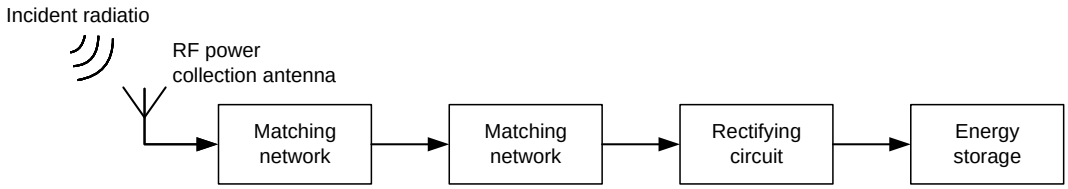

Figure 1.5: The typical block diagram of the energy harvesting model contains key components and steps [1].

studies [48, 49] on WPT systems adopt a linear model to focus on performance improvement with the help of energy scavenging.

2. **Non-linear EH model:** With further studies on the practical implementation of EH circuit [50], the results of experiment show the discrepancy between measured characteristics of EH circuit and calculated data from linear EH models is a huge gap, which would bring in resource allocation mismatches [51, 52]. To this end, the proposed non-linear EH model can capture the non-linear characteristics of the actual charging phenomenon in EH circuits.

In fact, employing the non-linear model to quantify energy conversion can significantly increase the computational complexity. A simple linear model is sufficient to analyze system performance which can contribute to a more simple resource allocation equation and programming in a low-power sensor communication system.

1.4.4 The Basic Concept of SWIPT

Based on the research of WPT and EH techniques, more sophisticated concepts are proposed to fully exploit the RF spectrum, such as wireless information transfer(WIT), wireless-powered communication (WPC), and wireless-powered backscatter communication (WPBC) [53]-[56]. In this regard, the heuristic combination of power and information transmission triggers further research on SWIPT system [1]. This technology allows the dual use of wave signal, not only for information decoding (ID) but also for energy harvesting (EH), resulting in giant progress in spectral efficiency and energy savings [57, 58]. However, two representative technical problems exist for the practical deployment of SWIPT system. The first-class problem is about propagation loss where the radio signal

with a short wavelength is extremely vulnerable to blockage in non-LoS paths and contributes to low efficient energy conversion [57]. Consequently, there is a need for employing the aforementioned IRS technology, as IRS can costume a more favorable propagation environment to circumvent heavily penetrate loss [11]. This benefit also motivates this thesis to focus on the new line of research on bridging SWIPT and IRS techniques.

Since information is destroyed directly after energy harvesting, the second challenge is how to accomplish both ID and EH on a same received signal [37]. For this reason, various types of energy splitting schemes have been proposed. Several receiver architectures for signal splitting are listed in the following.

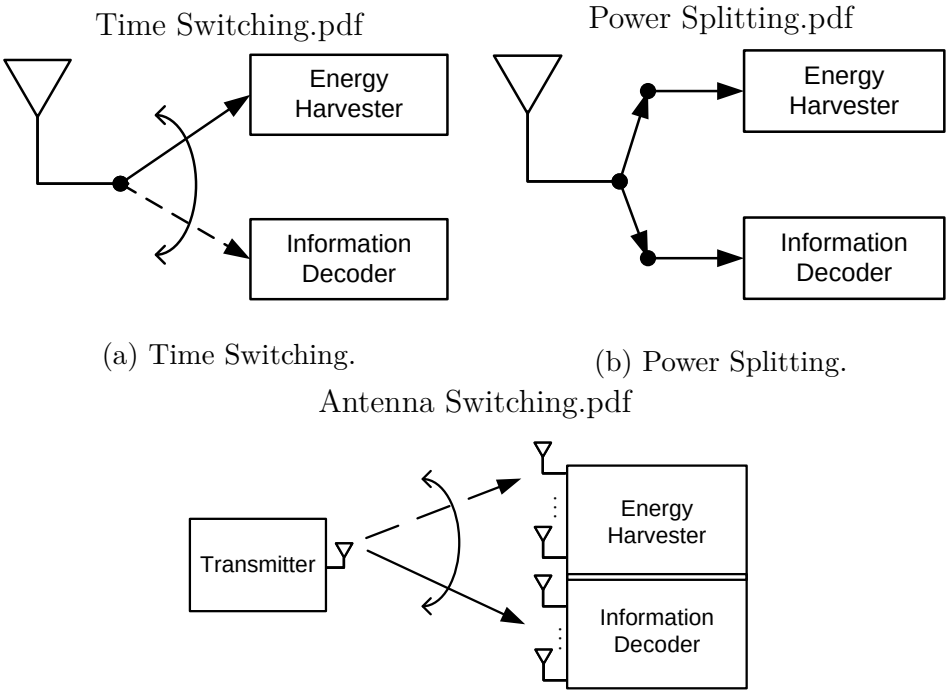

(a) Time Switching.

(b) Power Splitting.

(c) Antenna Switching.

Figure 1.6: Block diagram of three receiver structures for SWIPT system [2].

1. **Time Switching:** For time switching (TS) architectures, the transmission process is divided into different time slot [2], where the received signal is either used for convey information or energy scavenging, cf. Figure 1.6(a). The advantage of TS receivers is simple implementation and cheap hardware facility. In contrast, TS receiver requires stringent time synchronization.

2. **Power Splitting:** For power splitting (PS) architectures, the received wave can be split into two streams via a certain power splitting ratio, one part used for

energy supply; another part with conversion to information decoding, cf. Figure 1.6(b). Compared with TS receiver, this techniques contains complicated facilities and introduces extra optimization computation process about power splitting factor. However, PS receiver also provide accurate and instantaneous splitting effect especially for the delay-constraint system [2, 48].

3. **Antenna Switching:** For antenna switching (AS) architectures, some antennas are assigned as information decoding while some are the group for energy harvesting, cf. Figure 1.6(c). For optimal antenna assignment, dynamic programming is intractable process during each communication frame in terms of AS receiver [2].

1.5 Prior Works

The mMIMO, mmWave, and ultra-densification bring in numerous challenges to 5G even beyond 5G communication systems. Consequently, there are numerous research efforts have been devoted to designing useful solutions to aforementioned challenges. So far, the related promising solution designs are usually classified into two groups, one is based on SWIPT systems and another is based on IRS-aided SWIPT systems with different resource allocation schemes. At first, the authors of [59] and [60] proposed the SWIPT-based MISO and orthogonal frequency-division multiplexing (OFDM) communication networks to enhance energy efficiency, respectively. The energy consumption problem was further studied by [61] where artificial noise was incorporated to avoid information leakage to the potential eavesdroppers. Also, in [62], the author considered the energy fairness allocation for each receiver and developed the SDR algorithm for maximizing the minimum harvested energy. In practice, ID and EH may not be feasible from the same received signal. Nevertheless, some useful receiver architecture has been proposed to enable realize co-located receivers. For instance, a detailed performance analysis of co-located receivers with PS architecture was presented in [63] for SWIPT-based wireless network.

However, considering distance-related path loss and non-LoS signal attenuation would severely degrade RF signal power, the SWIPT system is not adequate to ensure the minimum harvested energy in practical situations. To overcome those bottlenecks, [64]-[68] proposed to incorporate IRS to expand the coverage. Specifically, the joint optimization

of beamforming vectors and reflect phase shift elements was studied in [69] to minimize transmit power in an IRS-assisted SWIPT system. Then in [65], the resource allocation study was extended to multiuser MIMO system, where AO was proposed for weighted sum-rate maximization. Since the resource allocation schemes in [65] were based on simple linear EH model, this model would not provide accurate charging service due to the non-linearity property in EH circuits. In contrast, [66] adopted the non-linear EH model that paves the way for matching the practical charging phenomenon at expense of computational complexity and efficiency. Then, in [67] and [68], the study was extended to co-lated receivers system with PS techniques. The prior works on this topic are summarized in Table 1.3.

1.6 Organization of the Thesis

Motivated by the prior works, this thesis considers IRS-aided wireless sensor networks incorporating the PS-based SWIPT system technique with a linear EH model and develop efficient resource allocation from the max-min rate fairness point of view to ensure data fairness among all the considered receivers. A brief overview of the rest of this thesis is illustrated as follows. In Chapter 2, we first propose a system model and then formulate the resource allocation algorithm design to maximize the minimum data rate in IRS-aided SWIPT system, which would be solved by the proposed algorithm in Chapter 3. Chapter 4 presents simulation results and verifies the functionality of incorporated IRS techniques to the system performance. In Chapter 5, we conclude with a brief summary of the results and give two direction of future works.

Table 1.3: The summary of prior works

Ref	Type of system	Objectives	Constraints	Solution Approaches
[59]	MISO-SWIPT	Minimize transmit power budget, and minimize interference -power-leakage-to-transmit -power ratio, maximize energy harvesting efficiency	QoS requirements	The semidefinite programming relaxation method
[60]	OFDM-SWIPT	Maximize energy efficiency	Minimum required data rate,maximum transmit power constraint	The iterative resource allocation method
[61]	MISO-SWIPT secure communication system	Maximize energy efficiency, and minimize total energy power	QoS requirements	The semidefinite programming relaxation method
[62]	MISO-SWIPT with max-min fairness protocal	Maximize the minimum harvested energy	Minimum required SINR, maximium tolerate channel capacity of energy receiver	The semidefinite programming relaxation method
[63]	MISO-SWIPT with co-located receivers	Minimize the total transmit power	Minimum required SINR, minimum harvested DC power	The semidefinite relaxation method
[69]	IRS-MISO-SWIPT with separated receivers and linear EH model	Minimize the total transmit power	QoS requirements,minimum harvested DC power	The penalty-based optimization method
[65]	IRS-MIMO-SWIPT with linear EH model	Maximize the weighted sum-rate	Minimum harvested DC power	The bisection search method, the successive convex approximation, the majorization-minimization method, the block coordinate descent algorithm
[66]	IRS-MISO-SWIPT secure communication system with non-linear EH model	Maximize the system sum-rate	Maximum transmit power budget, minimum harvested power, maximum tolerble information leakage	The alternating optimization method, the penalty-based method, the semidefinite relaxation method
[67]	IRS-MISO-SWIPT with co-located receivers and linear EH model	Maximize the energy efficiency indicator	Maximum transmit power constraint	The majorization-minimization method, the Dinkelbach method, the alternating optimization method, the semi-definite relaxation method
[68]	IRS-MISO-SWIPT with co-located receivers and non-linear EH model	Max-min energy efficiency	Minimum harvested DC power, maximum transmit power constraint, minimum required data rate	The majorization-minimization method, the penalty-based method, the alternating optimization method, the semi-definite relaxation method

Chapter 2

System Model and Problem Formulation

2.1 Signal Model

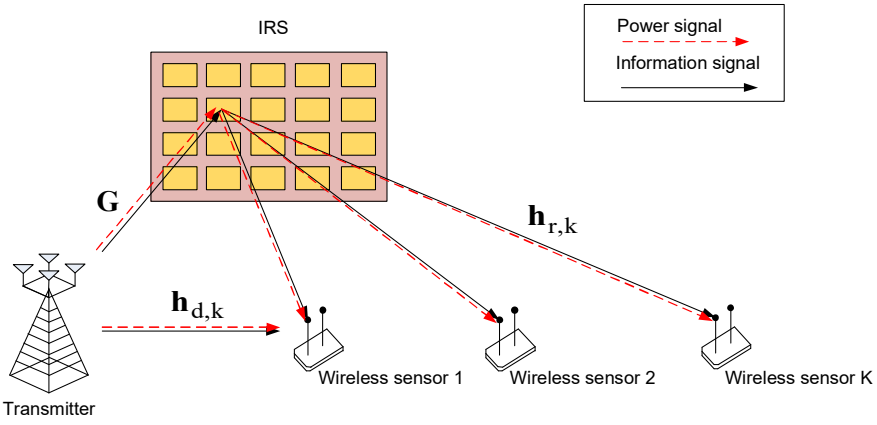

Model.pdf

Figure 2.1: Illustration of IRS-aided SWIPT model. There is one BS with N_{T} antennas and K wireless sensor as receiver equipped with a single antenna.

In this thesis, we consider an IRS-assisted wireless communication system where an IRS equipped with N reflecting elements enables the SWIPT process from BS with M transmitting antennas to K sets of low-power sensors. In particular, each sensor equipped with a single antenna. This system model is depicted in Figure 2.1. During each time

slot, the transmitted signal vector $\mathbf{x} \in \mathbb{C}^{N_\mathrm{T}}$ from the BS is given by:

$$\mathbf{x} = \underbrace{\sum_{k \in \mathcal{K}} \mathbf{w}_k s_k}_{\text{Information signals}} + \underbrace{\mathbf{w}_\mathrm{E}}_{\text{Energy signal}}, \tag{2.1}$$

where $\mathbf{w}_k \in \mathbb{C}^{N_\mathrm{T} \times 1}$ refers to the beamforming vector for sensor k and $\mathbf{w}_\mathrm{E} \in \mathbb{C}^{N_\mathrm{T} \times 1}$ stands for pseudo-random energy signal satisfying complex Gaussian distribution with zero mean and variance $\mathbf{W}_\mathrm{E}$, i.e., $\mathbf{w}_\mathrm{E} \sim \mathcal{CN}(0, \mathbf{W}_\mathrm{E})$. In particular, its covariance matrix $\mathbf{W}_\mathrm{E} \in \mathbb{H}^{N_\mathrm{T}}$ and $\mathbf{W}_\mathrm{E} \succeq \mathbf{0}$. We assume s_k denotes the encoded information signals assigned for sensor k. Without loss of generality, we assume s_k is independent and identically distributed (i.i.d.) and its energy is equal to one, denoted by expectation format $\mathbb{E}\left\{ \left| s_k^2 \right| \right\} = 1, \forall k \in \mathcal{K} = \{1, \ldots, K\}$.

2.2 IRS-aided System Channel Model

Two assumptions were adopted: one is that the channel of all sensors is a quasi-static flat fading channel [68]. The second assumption is that the channel state information (CSI)[1] for each transmission link is perfectly known at the BS and sensors. Then, the equivalent channel coefficient from the BS-to-IRS-to-sensor superimpose with the direct path from the BS-to-sensor could be written as:

$$\mathbf{h}_k^H = \underbrace{\mathbf{h}_{d,k}^H}_{\text{Direct path}} + \underbrace{\mathbf{h}_{r,k}^H \mathbf{\Phi} \mathbf{G}}_{\text{Reflected path}}. \tag{2.2}$$

In this representation, $\mathbf{h}_{d,k} \in \mathbb{C}^{N_\mathrm{T} \times 1}$, $\mathbf{h}_{r,k} \in \mathbb{C}^{N \times 1}$, $\mathbf{G} \in \mathbb{C}^{N \times N_\mathrm{T}}$ denote the direct channel vectors from the BS to sensor k, the reflected channel vectors from IRS to sensor k, and the channel equivalent gain from the BS to IRS, respectively. Besides, $\mathbf{\Phi} = \mathrm{diag}(\mathbf{v})$ with $\mathbf{v} = [e^{j\theta_1}, e^{j\theta_2}, \cdots, e^{j\theta_N}]^T$ are the reflection coefficient matrix at the IRS. In particular, $\theta_n \in [0, 2\pi]$ represent the phase shift of the n-th IRS element and all reflection amplitude are one[2] in this system model.

[1] Although the CSI is imperfect in practical systems, [70] proposed a novel approach successfully solve the channel estimation problem in multi-user IRS system. Thus, we assume perfect CSI for the design of resource allocation in this thesis.

[2] Note that this model representation of IRS is well-adopted in the literature and [19] demonstrate its advantage in intuitively exhibiting IRS basic properties.

2.3 SWIPT-based ID and EH Signal Model

The downlink received signal at sensor k is given by:

$$y_k = \mathbf{h}_k^H \sum_{k\in\mathcal{K}} \mathbf{w}_k s_k + \mathbf{h}_k^H \mathbf{w}_{\mathrm{E}} + n_k, \quad \forall k \in \mathcal{K}, \tag{2.3}$$

where n_k contains both the thermal noise and antenna noise originating from the receive antenna at the sensor k and they can be modeled as addictive white Gaussian noise (AWGN) with $n_k \sim \mathcal{CN}(0, \sigma_s^2)$. In particular, the PS receiver would be employed to separate the received signals into two power streams via the splitting ratio ρ_k $(0 \leq \rho_k \leq 1)$. In particular, the PS ratio ρ_k can adjust the proportion allocation to ID and EH parts. Accordingly, the signal received at each sensor k used in ID part is given by

$$\begin{aligned} y_k^{\mathrm{ID}} &= \sqrt{\rho_k}\left(\mathbf{h}_k^H \mathbf{x} + n_k\right) \\ &= \sqrt{\rho_k}\left(\mathbf{h}_k^H (\sum_{k\in\mathcal{K}} \mathbf{w}_k s_k + \mathbf{w}_{\mathrm{E}}) + n_k\right), \quad \forall k \in \mathcal{K}. \end{aligned} \tag{2.4}$$

On the other hand, the received signal at each sensor k used for energy harvesting is given by

$$\begin{aligned} y_k^{\mathrm{EH}} &= \sqrt{1-\rho_k}\left(\mathbf{h}_k^H \mathbf{x} + n_k\right) \\ &= \sqrt{1-\rho_k}\left(\mathbf{h}_k^H \sum_{k\in\mathcal{K}} \mathbf{w}_k s_k + \mathbf{h}_k^H \mathbf{w}_{\mathrm{E}} + n_k\right), \quad \forall k \in \mathcal{K}. \end{aligned} \tag{2.5}$$

2.4 Performance Metrics

As pseudo-random energy signal is known at each sensor where the interference regard of $\mathbf{w}_{\mathrm{E}}$ can be easily canceled out for ID parts [71], thereby signal-to-interference-noise ratio (SINR) at k-th sensor in terms of ID parts is given by[3]

$$\begin{aligned} \Gamma_k^{\mathrm{ID}} &= \frac{\rho_k \left|\mathbf{h}_k^H \mathbf{w}_k\right|^2}{\rho_k \left(\sum_{i\in\mathcal{K}\setminus\{k\}} \left|\mathbf{h}_k^H \mathbf{w}_i\right|^2\right) + \sigma_{\mathrm{s}}^2} \\ &= \frac{\left|\mathbf{w}_k^H \mathbf{H}_k \mathbf{w}_k\right|^2}{\sum_{i\in\mathcal{K}\setminus\{k\}} \left|\mathbf{h}_k^H \mathbf{w}_i\right|^2 + \frac{\sigma_{\mathrm{s}}^2}{\rho_k}}, \quad \forall k \in \mathcal{K}, \end{aligned} \tag{2.6}$$

where the channel vector is defined by $\mathbf{H}_k = \mathbb{E}\{\mathbf{h}_k^H \mathbf{h}_k\}$ and σ_s^2 refers to the signal processing noise power at sensors. Accordingly, the individual achievable data rate is given

[3]Note that the authors in [72] also proposed related algorithms to enable the cancellation of interference from energy signal, thereby this representation of SINR is valid.

by

$$R_k = \log_2\left(1+\Gamma_k^{\mathrm{ID}}\right), \quad \forall k \in \mathcal{K}. \tag{2.7}$$

More importantly, since the EH model can approximate the relationship between input and output with extremely less computation complexity, the simple linear EH model is adopted. Therefore, the harvested power at k-th sensor can be written as:

$$\begin{aligned} \Phi_k^{\mathrm{EH}} &= \eta_k P_k^{\mathrm{EH}} \quad \text{where} \\ P_k^{\mathrm{EH}} &= (1-\rho_k)\mathbb{E}\left\{\sum_{i\in\mathcal{K}}\left|\mathbf{h}_k^H\mathbf{w}_i\right|^2 + |\mathbf{h}_k^H\mathbf{w}_{\mathrm{E}}|^2\right\} \\ &= (1-\rho_k)\left(\sum_{i\in\mathcal{K}}\mathbf{w}_i^H\mathbf{H}_k\mathbf{w}_i + \mathrm{Tr}\ (\mathbf{H}_k\mathbf{W}_{\mathrm{E}})\right), \quad \forall k \in \mathcal{K}. \end{aligned} \tag{2.8}$$

In (2.8), $\eta_k \in [0,1]$ stands for the fixed energy conversion efficiency of sensor k. Considering the noise power from signal processing is smaller than harvesting energy power, thus we ignore the power of receiver noise in (2.8) [37].

2.5 Problem Formulation

In this section, we aim to achieve the fair data rate among users with the constraints of QoS. As such, the optimization objectives can be formulated as:

$$\begin{aligned} \underset{\rho_k,\mathbf{w}_k,\mathbf{\Phi},\mathbf{W}_{\mathrm{E}}}{\text{maximize}} \quad & \min_k\{R_k(\rho_k,\mathbf{w}_k,\mathbf{\Phi},\mathbf{W}_{\mathrm{E}})\} \\ \text{subject to} \quad & \mathrm{C1}: \textstyle\sum_{k\in\mathcal{K}}\|\mathbf{w}_k\|^2 + \mathrm{Tr}\,(\mathbf{W}_{\mathrm{E}}) \le P_{\max}, \\ & \mathrm{C2}: \Gamma_k^{\mathrm{ID}} \ge \Gamma_{k,\mathrm{req}}, \quad \forall k, \\ & \mathrm{C3}: P_k \ge P_{k,\mathrm{req}}, \quad \forall k, \\ & \mathrm{C4}: |\mathbf{\Phi}_{nn}| = 1, \quad \forall n \\ & \mathrm{C5}: 0 \le \rho_k \le 1, \quad \forall k, \end{aligned} \tag{2.9}$$

where $P_{\max}$ in C1 refers to maximum transmit power budget constraint at the BS. Constraint C2 can ensure QoS services for each sensor k with respect to SINR. $P_{k,\mathrm{req}}$ in constraint C3 guarantees the minimum harvesting energy for individual user k. Constraint C4 refers that the reflected elements on IRS have unit modulus components and constraint C5 is the boundary for the power splitting ratio variable. The formulated optimization problem (2.9) is not a standard form of convex problems. In particular, the optimization variables $\{\mathbf{w}_k, \rho_k, \mathbf{W}_{\mathrm{E}}\}$ are coupled with phase shift $\mathbf{\Phi}$ in constraints C2

and C3. Besides, the unit modulus in C4 obviously is a non-convex constraint as well. Although there are no accessible tools to tackle non-convex problems, we can convert them into equivalent tractable convex problems by proposing some effective algorithms.

Chapter 3

Solution of the Optimization Problem

3.1 Algorithm Design

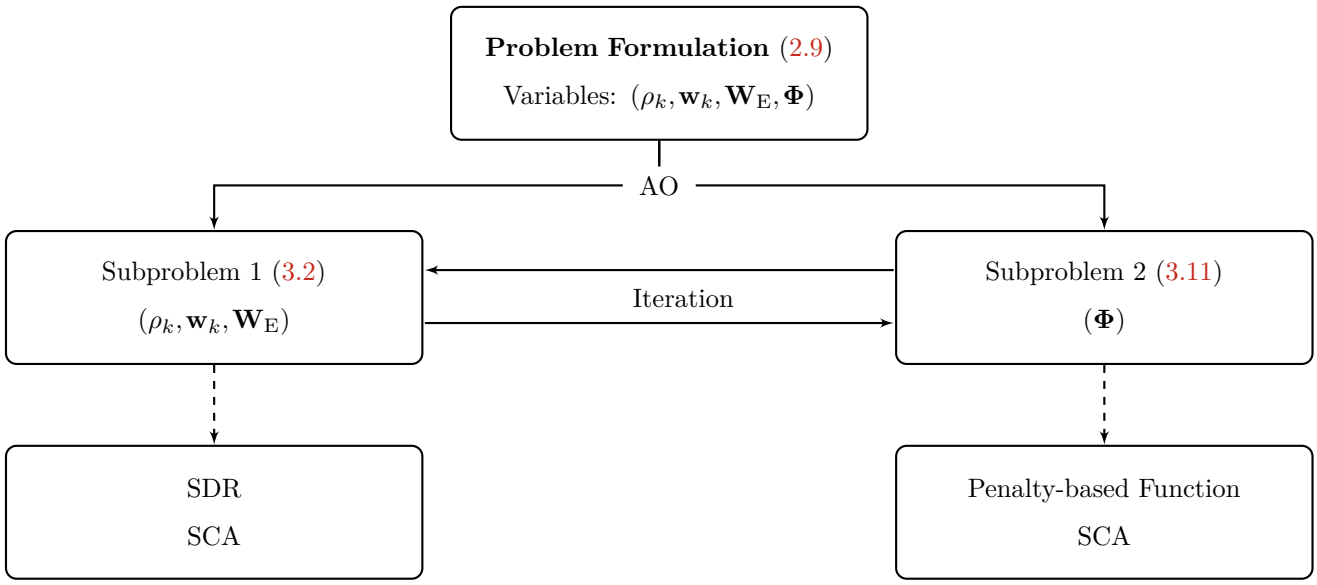

Figure 3.1: Flow chart of the proposed algorithm for solving the non-convex problem.

In this chapter, we prepare to solve the aforementioned problem in (2.9). Although the objective function follows the standard form of optimization problem, the coupling of those optimization variables contributes to highly non-convexity. In this regard, we adopt AO method to implement alternate optimization in terms of $\{\rho_k, \mathbf{w}_k, \mathbf{W}_{\mathrm{E}}\}$ and $\{\mathbf{\Phi}\}$ respectively [27]. When the optimization variables are split via AO method, the problem

in (2.9) would yield two subproblems, where each subproblem has only one grouped variable and other grouped variable is at a feasible value. For the first subproblem with variables $\{\rho_k, \mathbf{w}_k, \mathbf{W}_{\mathrm{E}}\}$, we adopt the first-order Taylor approximation [73] to rewrite the data rate and adopt SDR to handle the non-convexity from the rank-one constraint. In terms of the second subproblem with variables $\mathbf{\Phi}$, we apply another method, i.e., the penalty method [74, 75], to release the rank-one constraint and apply the same SCA algorithm to optimize the phase shift. Finally, the final optimal solution can be obtained by separately and alternatively updating these two grouped optimization variables via two subproblems. The proposed algorithm is summarized in Figure 3.1.

3.2 Alternative Optimization

First, we transform the objection function into its equivalent problem formulation, i.e., the epigraph problem form [76] via an auxiliary variable. Based on the concept of epigraph where epigraph function preserves convexity, the equivalent objective function of (2.9) can be formulated as follows

$$
\begin{aligned}
&\underset{\tau_k,\rho_k,\mathbf{w}_k,\mathbf{\Phi},\mathbf{W}_{\mathrm{E}}}{\text{maximize}} \quad \tau_k \\
&\text{subject to} \quad \mathrm{C1}: \textstyle\sum_{k\in\mathcal{K}} \|\mathbf{w}_k\|^2 + \mathrm{Tr}\left(\mathbf{W}_{\mathrm{E}}\right) \leq P_{\max}, \\
&\qquad\qquad \mathrm{C2}: \Gamma_k \geq \Gamma_{k,\mathrm{req}}, \quad \forall k, \\
&\qquad\qquad \mathrm{C3}: P_k \geq P_{k,\mathrm{req}}, \quad \forall k, \\
&\qquad\qquad \mathrm{C4}: |\mathbf{\Phi}_{nn}| = 1, \quad \forall n, \\
&\qquad\qquad \mathrm{C5}: 0 \leq \rho_k \leq 1, \quad \forall k, \\
&\qquad\qquad \mathrm{C6}: \tau_k - R_k(\rho_k, \mathbf{w}_k, \Phi, \mathbf{W}_{\mathrm{E}}) \leq 0, \quad \forall k,
\end{aligned}
\tag{3.1}
$$

where τ_k is the auxiliary optimization variables. Although the objective function follows the standard form of optimization problem, the coupling of those optimization variables contributes to highly non-convexity.

In this regard, we adopt the AO method to alternately find the optimal solution for beamforming vector $\mathbf{w}_k$ and phase shift matrix $\mathbf{\Phi}$ while holding the other variables at a feasible value. The problem in (3.1) would yield two subproblems, one is beamforming optimization problem with respect to $\{\mathbf{w}_k, \rho_k\}$ and another is phase shift optimization problem with respect to $\mathbf{\Phi}$.

3.3 Subproblem 1: Optimization of Beamforming and PS Ratio

When we settle phase shift $\mathbf{\Phi}$ into a fixed stationary point via AO algorithm, we can recast the original problem formulation in (3.1) as follows

$$\begin{aligned}
&\underset{\tau_k,\rho_k,\mathbf{W}_k,\mathbf{W}_{\mathrm{E}}}{\text{maximize}} \quad \tau_k \\
&\text{subject to} \quad \mathrm{C1}: \textstyle\sum_{k\in\mathcal{K}} \mathrm{Tr}\left(\mathbf{W}_k\right) + \mathrm{Tr}\left(\mathbf{W}_{\mathrm{E}}\right) \le P_{\max}, \\
&\qquad\qquad \mathrm{C2}: \Gamma_k^{\mathrm{ID}} \ge \Gamma_{k,\mathrm{req}}, \quad \forall k, \\
&\qquad\qquad \mathrm{C3}: P_k \ge P_{k,\mathrm{req}}, \quad \forall k, \\
&\qquad\qquad \mathrm{C5}: 0 \le \rho_k \le 1, \quad \forall k, \\
&\qquad\qquad \mathrm{C6}: \tau_k - R_k(\rho_k, \mathbf{W}_k, \mathbf{W}_{\mathrm{E}}) \le 0, \quad \forall k, \\
&\qquad\qquad \mathrm{C7}: \mathrm{Rank}(\mathbf{W}_k) \le 1, \quad \forall k, \\
&\qquad\qquad \mathrm{C8}: \mathbf{W}_k \succeq \mathbf{0}, \quad \forall k,
\end{aligned} \tag{3.2}$$

where $\mathbf{W}_k = \mathbf{w}_k^H \mathbf{w}_k$ and the constraints C7 and C8 in problem (3.2) are able to ensure this replacement is valid even after optimizing $\mathbf{W}_k$.

To further solve the non-convexity, we propose some transformation and manipulations and the problem in (3.2) can be written as

$$\begin{aligned}
&\underset{\tau_k,\rho_k,\mathbf{W}_k,\mathbf{W}_{\mathrm{E}}}{\text{maximize}} \quad \tau_k \\
&\text{subject to} \quad \mathrm{C1}: \textstyle\sum_{k\in\mathcal{K}} \mathrm{Tr}\left(\mathbf{W}_k\right) + \mathrm{Tr}\left(\mathbf{W}_{\mathrm{E}}\right) \le P_{\max}, \\
&\qquad\qquad \mathrm{C2}: \frac{\mathrm{Tr}(\mathbf{H}_k\mathbf{W}_k)}{\sum_{i\in\mathcal{K}\setminus\{k\}} \mathrm{Tr}(\mathbf{H}_k\mathbf{W}_i) + \frac{\sigma_{\mathbf{s}}^2}{\rho_k}} \ge \Gamma_{k,\mathrm{req}}, \quad \forall k, \\
&\qquad\qquad \mathrm{C3}: \textstyle\sum_{i\in\mathcal{K}} \mathrm{Tr}(\mathbf{H}_k\mathbf{W}_i) + \mathrm{Tr}\ \left(\mathbf{H}_k\mathbf{W}_{\mathrm{E}}\right) \ge \frac{P_{k,\mathrm{req}}}{\eta(1-\rho_k)}, \\
&\qquad\qquad \mathrm{C5}: 0 \le \rho_k \le 1, \quad \forall k, \\
&\qquad\qquad \mathrm{C6}: \tau_k \le \log_2\left(1 + \frac{\mathrm{Tr}(\mathbf{H}_k\mathbf{W}_k)}{\sum_{i\in\mathcal{K}\setminus\{k\}} \mathrm{Tr}(\mathbf{H}_k\mathbf{W}_i) + \frac{\sigma_{\mathbf{s}}^2}{\rho_k}}\right), \\
&\qquad\qquad \mathrm{C7}: \mathrm{Rank}(\mathbf{W}_k) \le 1, \quad \forall k, \\
&\qquad\qquad \mathrm{C8}: \mathbf{W}_k \succeq \mathbf{0}, \quad \forall k.
\end{aligned} \tag{3.3}$$

As shown in problem (3.3), C6 and C7 contribute to non-convexity. Obviously, C2, C3 is a convex constraint in relate to ρ_k due to the inverse function, i.e., $\frac{1}{1-\rho_k}$, is convex for $0 \le \rho_k \le 1$. To leverage the solvable convex optimization design, we first tackle the non-convexity of C6 based on SCA techniques, then we relax the constraint C7 based on

the concept of SDR [66, 74, 75]. To tackle the non-convexity in C6, data rate R_k can be converted to a more tractable form as follows

$$\begin{aligned} R_k &= \log_2\left(1+\frac{\mathrm{Tr}(\mathbf{H}_k\mathbf{W}_k)}{\sum_{i\in\mathcal{K}\setminus\{k\}}\mathrm{Tr}(\mathbf{H}_k\mathbf{W}_i)+\frac{\sigma_{\mathbf{s}}^2}{\rho_k}}\right) \\ &= \log_2\left(\frac{\mathrm{Tr}(\mathbf{H}_k\mathbf{W}_k)+\sum_{i\in\mathcal{K}\setminus\{k\}}\mathrm{Tr}(\mathbf{H}_k\mathbf{W}_i)+\frac{\sigma_{\mathbf{s}}^2}{\rho_k}}{\sum_{i\in\mathcal{K}\setminus\{k\}}\mathrm{Tr}(\mathbf{H}_k\mathbf{W}_i)+\frac{\sigma_{\mathbf{s}}^2}{\rho_k}}\right) \\ &= \log_2\left(\mathrm{Tr}(\mathbf{H}_k\mathbf{W}_k)+\sum_{i\in\mathcal{K}\setminus\{k\}}\mathrm{Tr}(\mathbf{H}_k\mathbf{W}_i)+\frac{\sigma_{\mathbf{s}}^2}{\rho_k}\right)-\log_2\left(\sum_{i\in\mathcal{K}\setminus\{k\}}\mathrm{Tr}(\mathbf{H}_k\mathbf{W}_i)+\frac{\sigma_{\mathbf{s}}^2}{\rho_k}\right). \end{aligned} \tag{3.4}$$

For the sake of notational simplicity, we define two auxiliary variables to rewrite equation (3.4) as follows

$$\begin{aligned} R_k &= \underbrace{A_1}_{\text{concave}}\underbrace{-B_1}_{\text{convex}}, \quad \text{where} \\ A_1 &= \log_2\left(\mathrm{Tr}(\mathbf{H}_k\mathbf{W}_k)+\sum_{i\in\mathcal{K}\setminus\{k\}}\mathrm{Tr}(\mathbf{H}_k\mathbf{W}_i)+\frac{\sigma_{\mathbf{s}}^2}{\rho_k}\right), \\ B_1 &= \log_2\left(\sum_{i\in\mathcal{K}\setminus\{k\}}\mathrm{Tr}(\mathbf{H}_k\mathbf{W}_i)+\frac{\sigma_{\mathbf{s}}^2}{\rho_k}\right). \end{aligned} \tag{3.5}$$

Although A_1 is the concave function and $-B_1$ is the convex function in terms of ρ_k and $\mathbf{W}_k$, the combination of A_1 and $-B_1$ does not preserve convexity. If we replace one concave function with a constant number, the new combination the logarithmic function subtract a constant is an affine operation that preserves the convexity. In this regard, the upper bound bound for the logarithmic function B_1 can be obtained by the utilization of SCA method [73, 77]. More precisely, the upper bound could be expressed through the first-order Taylor approximation as follows

$$\begin{aligned} &B_1\left(\mathbf{W}_k,\rho_k\right)\le B_1\left(\mathbf{W}_k^{(t)},\rho_k^{(t)}\right)+\mathrm{Tr}\left(\nabla_{\mathbf{W}_k}^H B_1\left(\mathbf{W}_k^{(t)},\rho_k^{(t)}\right)(\mathbf{W}_k-\mathbf{W}_k^{(t)})\right) \\ &+\mathrm{Tr}\left(\partial_{\rho_k}^H B_1\left(\mathbf{W}_k^{(t)},\rho_k^{(t)}\right)(\rho_k-\rho_k^{(t)})\right)\triangleq\tilde{B}_1(\mathbf{W}_k,\rho_k), \end{aligned} \tag{3.6}$$

where superscript (t) refers to the iteration index. $\mathbf{W}_k^{(t)}$ and $\rho_k^{(t)}$ refers to the feasible solution at the t-th iteration, respectively. The first-order derivative function of B_k can be given as

$$\nabla_{\mathbf{W}_k}B_1\left(\mathbf{W}_k,\rho_k\right)=\frac{\mathbf{H}_k}{\ln 2\left(\sum_{i\in\mathcal{K}\setminus\{k\}}\mathrm{Tr}(\mathbf{H}_k\mathbf{W}_i)+\frac{\sigma_s^2}{\rho_k}\right)}, \tag{3.7}$$

$$\partial_{\rho_k}B_1\left(\mathbf{W}_k,\rho_k\right)=-\frac{\sigma_s^2(\rho_k)^{-2}}{\ln 2\left(\sum_{i\in\mathcal{K}\setminus\{k\}}\mathrm{Tr}(\mathbf{H}_k\mathbf{W}_i)+\frac{\sigma_s^2}{\rho_k}\right)}. \tag{3.8}$$

So far, the remaining non-convexity is due to the presence of C7, which is a major contributing factor to the problem (3.3) that cannot be solved in nondeterministic polynomial time [78]. Accordingly, we can relax the rank-one matrix constraint and the problem (3.3) would become a standard semidefinite programming (SDP) problem, where the convex program solvers, such as CVX, can resolve it. With the tight convex lower bound for the logarithmic function B_1, problem (3.3) can be rewritten as

$$\begin{aligned}
\underset{\tau_k,\rho_k,\mathbf{W}_k,\mathbf{W}_{\mathrm{E}}}{\text{maximize}} \quad & \tau_k \\
\text{subject to} \quad & \mathrm{C1}: \textstyle\sum_{k\in\mathcal{K}} \mathrm{Tr}\left(\mathbf{W}_k\right) + \mathrm{Tr}\left(\mathbf{W}_{\mathrm{E}}\right) \le P_{\max}, \\
& \mathrm{C2}: \tfrac{\mathrm{Tr}(\mathbf{H}_k\mathbf{W}_k)}{\Gamma_{k,\mathrm{req}}} - \textstyle\sum_{i\in\mathcal{K}\setminus\{k\}} \mathrm{Tr}\left(\mathbf{H}_k\mathbf{W}_i\right) \ge \tfrac{\sigma_s^S}{\rho_k}, \quad \forall k, \\
& \mathrm{C3}: \textstyle\sum_{i\in\mathcal{K}} \mathrm{Tr}(\mathbf{H}_k\mathbf{W}_i) + \mathrm{Tr}\ \left(\mathbf{H}_k\mathbf{W}_{\mathrm{E}}\right) \ge \tfrac{P_{k,\mathrm{req}}}{\eta(1-\rho_k)}, \\
& \mathrm{C5}: 0 \le \rho_k \le 1, \quad \forall k, \\
& \mathrm{C6}: \tau_k \le A_1 - \mathrm{Tr}\left(B_1\left(\mathbf{W}_k^{(t)}, \rho_k^{(t)}\right)\right) \\
& \qquad - \textstyle\sum_{k\in\mathcal{K}} \mathrm{Tr}\left(\nabla^H_{\mathbf{W}_k} B_1\left(\mathbf{W}_k^{(t)}, \rho_k^{(t)}\right)\left(\mathbf{W}_k - \mathbf{W}_k^{(t)}\right)\right) \\
& \qquad - \mathrm{Tr}\left(\nabla^H_{\rho_k} B_1\left(\mathbf{W}_k^{(t)}, \rho_k^{(t)}\right)\left(\rho_k - \rho_k^{(t)}\right)\right), \\
& \mathrm{C8}: \mathbf{W}_k \succeq \mathbf{0}, \quad \forall k.
\end{aligned} \tag{3.9}$$

For the sake of presentation, we do not write out the variables $\{\mathbf{W}_k^{(t)}, \rho_k^{(t)}\}$ inside the gradient function and neglect the irrelevant constant terms, i.e. $\mathrm{Tr}\left(B_1\left(\mathbf{W}_k^{(t)}, \rho_k^{(t)}\right)\right)$, $-\nabla^H_{\mathbf{W}_k} B_1\left(\mathbf{W}_k^{(t)}, \rho_k^{(t)}\right)\mathbf{W}_k^{(t)}$ and $-\nabla^H_{\rho_k} B_1\left(\mathbf{W}_k^{(t)}, \rho_k^{(t)}\right)\rho_k^{(t)}$ as follows

$$\begin{aligned}
\underset{\tau_k,\rho_k,\mathbf{W}_k,\mathbf{W}_{\mathrm{E}}}{\text{maximize}} \quad & \tau_k \\
\text{subject to} \quad & \mathrm{C1}: \textstyle\sum_{k\in\mathcal{K}} \mathrm{Tr}\left(\mathbf{W}_k\right) + \mathrm{Tr}\left(\mathbf{W}_{\mathrm{E}}\right) \le P_{\max}, \\
& \mathrm{C2}: \tfrac{\mathrm{Tr}(\mathbf{H}_k\mathbf{W}_k)}{\Gamma_{k,\mathrm{req}}} - \textstyle\sum_{i\in\mathcal{K}\setminus\{k\}} \mathrm{Tr}\left(\mathbf{H}_k\mathbf{W}_i\right) \ge \tfrac{\sigma_s^S}{\rho_k}, \quad \forall k, \\
& \mathrm{C3}: \textstyle\sum_{i\in\mathcal{K}} \mathrm{Tr}(\mathbf{H}_k\mathbf{W}_i) + \mathrm{Tr}\ \left(\mathbf{H}_k\mathbf{W}_{\mathrm{E}}\right) \ge \tfrac{P_{k,\mathrm{req}}}{\eta(1-\rho_k)}, \\
& \mathrm{C5}: 0 \le \rho_k \le 1, \quad \forall k, \\
& \mathrm{C6}: \tau_k \le A_1 - \textstyle\sum_{k\in\mathcal{K}} \mathrm{Tr}\left(\mathbf{W}_k\nabla^H_{\mathbf{W}_k} B_1\right) - \mathrm{Tr}\left(\rho_k\nabla^H_{\rho_k} B_1\right), \quad \forall k, \\
& \mathrm{C8}: \mathbf{W}_k \succeq \mathbf{0}, \quad \forall k.
\end{aligned} \tag{3.10}$$

However, when we directly remove this rank-one constraint, two cases of solution would exist for the obtained problem formulation. If the final solution for $\mathbf{W}_k$ satisfies constraint C7 in problem (3.3), then we can perform the eigenvalue decomposition (EVD) to obtain the optimal beamforming $\mathbf{w}_k$ based on the equivalent optimization problem in (3.10),

where same method is normally adopted in literatures, e.g. [77], [79], [80]. Another case is the obtained matrix $\mathbf{W}_k$ with $\text{Rank}(\mathbf{W}_k) > 1$, then the value of $\mathbf{w}_k$ after EVD computation on $\mathbf{W}_k$ is not a feasible solution.

Algorithm 1 SDR-Based SCA Algorithm

1: Assume iteration index $l = 1$
2: Relax the rank-one constraint via SDR
3: **repeat**
4: Solve relaxed version problem (3.10) for given $\{\rho_k^{(l)}, \mathbf{W}_k^{(l)}, \mathbf{W}_{\text{E}}^{(l)}\}$ to update $\{\rho_k^{(l+1)}, \mathbf{W}_k^{(l+1)}, \mathbf{W}_{\text{E}}^{(l+1)}\}$
5: Set $l = l + 1$ and update the optimization variables
6: **until** convergence
7: Obtain $\{\rho_k^\star, \mathbf{W}_k^\star, \mathbf{W}_{\text{E}}^\star\} = \{\rho_k^{(l)}, \mathbf{W}_k^{(l)}, \mathbf{W}_{\text{E}}^{(l)}\}$

Therefore, if the tightness of the relaxation could be guaranteed, the rank-one constraint would not be considered. In fact, the following important Theorem 1 reveals the sufficient condition for semidefinite programming relaxation.

Theorem 1. When the channel vectors $\mathbf{h}_k$ are statistically independent and the considered problem formulation is feasible, the optimal beamforming matrix $\mathbf{W}_k$ of problem (3.9) would be rank-one matrix for any sensor k.

Proof. Please refer to Appendix A for a proof of Theorem 1. ■

By utilizing the **Algorithm 1**, the iterative optimal solutions $\{\rho_k^\star, \mathbf{W}_k^\star, \mathbf{W}_{\text{E}}^\star\}$ can be obtained. Since the relaxed version of proposed problem (3.10) belongs to a typical SDP problem, the SDR-based SCA algorithm is guaranteed to converge to local optimal solution [76].

3.4 Subproblem 2: Optimization of Phase Shift

Based on the optimization results of $\{\mathbf{W}_k^\star, \mathbf{W}_{\text{E}}^\star, \rho_k^\star\}$, the concerned optimization problem formulation with coupled variables can be simplified. In other words, we only search for the optimal solution of the phase shift matrix without the interference from other

variables. Under given $\{\mathbf{W}_k^\star, \mathbf{W}_{\mathrm{E}}^\star, \rho_k^\star\}$, the problem (3.1) can be recast as follows

$$\begin{aligned} \underset{\tau_k, \mathbf{\Phi}}{\text{maximize}} \quad & \tau_k \\ \text{subject to} \quad & \mathrm{C2}: \Gamma_k \geq \Gamma_{k,\mathrm{req}}, \quad \forall k, \\ & \mathrm{C3}: P_k \geq P_{k,\mathrm{req}}, \quad \forall k, \\ & \mathrm{C4}: |\mathbf{\Phi}_{nn}| = 1, \quad \forall n, \\ & \mathrm{C6}: \tau_k - R_k(\Phi) \leq 0, \quad \forall k. \end{aligned} \tag{3.11}$$

In order to further exploit the optimization variables $\mathbf{\Phi}$, we can separate it from the expression of (2.2) and reexpress this formula in vector form as follows

$$\mathbf{h}_k^H = \mathbf{h}_{d,k}^H + \mathbf{h}_{r,k}^H \mathbf{\Phi} \mathbf{G} = \mathbf{h}_{d,k}^H + \mathbf{v}^T \operatorname{diag}(\mathbf{h}_{r,k}^H) \mathbf{G} = \tilde{\mathbf{v}}^T \mathbf{L}_k, \tag{3.12}$$

where $\tilde{\mathbf{v}} = \begin{bmatrix} \mathbf{v}^T & 1 \end{bmatrix}^T \in \mathbb{C}^{(N+1)\times 1}$ and $\mathbf{L}_k = \begin{bmatrix} \left(\operatorname{diag}(\mathbf{h}_{r,k}^H)\mathbf{G}\right)^T & \mathbf{h}_{d,k}^* \end{bmatrix}^T \in \mathbb{C}^{(N+1)\times N_{\mathrm{T}}}$. With $\mathbf{V} = \tilde{\mathbf{v}}\tilde{\mathbf{v}}^H \in \mathbb{C}^{(N+1)\times(N+1)}$, we have

$$\begin{aligned} \left|\mathbf{h}_k^H \mathbf{w}_k\right|^2 &= \mathbf{w}_k^H \mathbf{h}_k \mathbf{h}_k^H \mathbf{w}_k = \mathbf{w}_k^H \tilde{\mathbf{v}} \mathbf{L}_k \mathbf{L}_k^H \tilde{\mathbf{v}}^H \mathbf{w}_k = \operatorname{Tr}\left(\mathbf{L}_k \mathbf{V} \mathbf{L}_k^H \mathbf{W}_k\right) \\ &= \operatorname{Tr}\left(\mathbf{M}_k \mathbf{W}_k\right), \end{aligned} \tag{3.13}$$

where $\mathbf{M}_k = \mathbf{L}_k \mathbf{V} \mathbf{L}_k^H$. In addition, problem formulation (3.11) can be recast as

$$\begin{aligned} \underset{\tau_k, \mathbf{V}}{\text{maximize}} \quad & \tau_k \\ \text{subject to} \quad & \mathrm{C2}: \frac{\operatorname{Tr}(\mathbf{M}_k \mathbf{W}_k)}{\sum_{i\in\mathcal{K}\setminus\{k\}} \operatorname{Tr}(\mathbf{M}_k \mathbf{W}_i) + \frac{\sigma_{\mathbf{s}}^2}{\rho_k}} \geq \Gamma_{k,\mathrm{req}}, \quad \forall k, \\ & \mathrm{C3}: \textstyle\sum_{i\in\mathcal{K}} \operatorname{Tr}(\mathbf{M}_k \mathbf{W}_i) + \operatorname{Tr}\ (\mathbf{M}_k \mathbf{W}_{\mathrm{E}}) \geq \frac{P_{k,\mathrm{req}}}{\eta(1-\rho_k)}, \\ & \mathrm{C4}: \operatorname{Diag}(\mathbf{V}) = \mathbf{1}_{N+1}, \\ & \mathrm{C6}: \tau_k - R_k(\mathbf{V}) \leq 0, \quad \forall k, \\ & \mathrm{C9}: \mathbf{V} \succeq \mathbf{0}, \\ & \mathrm{C10}: \operatorname{Rank}(\mathbf{V}) \leq 1, \end{aligned} \tag{3.14}$$

where C9 and C10 are imposed to ensure the equation $\mathbf{V} = \tilde{\mathbf{v}}\tilde{\mathbf{v}}^H$ holds after optimization. Due to the existence of C6 and C10, (3.14) is a non-convex problem. Following the same process of the aforementioned methods in (3.6), we adopt the first-order Taylor approximation to rewrite the data rate as follows

$$\begin{aligned} R_k &= \log_2\left(\operatorname{Tr}(\mathbf{M}_k \mathbf{W}_k) + \sum_{i\in\mathcal{K}\setminus\{k\}} \operatorname{Tr}(\mathbf{M}_k \mathbf{W}_i) + \frac{\sigma_{\mathbf{s}}^2}{\rho_k}\right) - \log_2\left(\sum_{i\in\mathcal{K}\setminus\{k\}} \operatorname{Tr}(\mathbf{M}_k \mathbf{W}_i) + \frac{\sigma_{\mathbf{s}}^2}{\rho_k}\right), \\ &= A_2(\mathbf{V}) - B_2(\mathbf{V}), \end{aligned} \tag{3.15}$$

where,

$$
\begin{aligned}
A_2(\mathbf{V}) &= \log_2\left(\mathrm{Tr}(\mathbf{M}_k\mathbf{W}_k) + \sum_{i\in\mathcal{K}\setminus\{k\}} \mathrm{Tr}(\mathbf{M}_k\mathbf{W}_i) + \frac{\sigma_{\mathbf{s}}^2}{\rho_k}\right), \\
B_2(\mathbf{V}) &= \log_2\left(\sum_{i\in\mathcal{K}\setminus\{k\}} \mathrm{Tr}(\mathbf{M}_k\mathbf{W}_i) + \frac{\sigma_{\mathbf{s}}^2}{\rho_k}\right).
\end{aligned} \tag{3.16}
$$

Furthermore,

$$
B_2(\mathbf{V}) \le B_2(\mathbf{V}^{(t)}) + \mathrm{Tr}\left(\nabla_{\mathbf{V}}^H B_2(\mathbf{V}-\mathbf{V}^{(t)})\right) \triangleq \tilde{B}_2(\mathbf{V}). \tag{3.17}
$$

Next, we would handle the non-convexity from constraint C10 based on the penalty-based method[4] as in [74, 75]. According to the linear algebra knowledge, we have the nuclear norm as $\|\mathbf{X}\|_* = \sum_i \sigma_i$, where σ_i denotes i-th singular value of X, and the Euclidean norm as $\|\mathbf{X}\|_2 = \max_i\{\sigma_i\}$. It can be observed that $\|\mathbf{X}\|_* \ge \|\mathbf{X}\|_2$, where the equality holds only with the rank-one matrix. Consequently, we can rewrite the constraint C10 as follows

$$
\mathrm{Rank}(\mathbf{V}) \le 1 \Rightarrow \|\mathbf{V}\|_* - \|\mathbf{V}\|_2 \le 0. \tag{3.18}
$$

When we impose the penalty term, i.e., (3.18) into the objective function, the rank-one constraint can be cancelled. Thus, problem (3.14) can be expressed as

$$
\begin{aligned}
\underset{\mathbf{V}}{\text{minimize}} \quad & \frac{1}{\mu}\left(\|\mathbf{V}\|_* - \|\mathbf{V}\|_2\right) \\
\text{subject to} \quad & \mathrm{C2}: \frac{\mathrm{Tr}(\mathbf{M}_k\mathbf{W}_k)}{\sum_{i\in\mathcal{K}\setminus\{k\}}\mathrm{Tr}(\mathbf{M}_k\mathbf{W}_i)+\frac{\sigma_{\mathbf{s}}^2}{\rho_k}} \ge \Gamma_{k,\mathrm{req}}, \quad \forall k, \\
& \mathrm{C3}: \textstyle\sum_{i\in\mathcal{K}}\mathrm{Tr}(\mathbf{M}_k\mathbf{W}_i) + \mathrm{Tr}\ (\mathbf{M}_k\mathbf{W}_{\mathrm{E}}) \ge \frac{P_{k,\mathrm{req}}}{\eta(1-\rho_k)}, \\
& \mathrm{C4}: \mathrm{Diag}(\mathbf{V}) = \mathbf{1}_{N+1}, \\
& \mathrm{C6}: \tau_k - A_2(\mathbf{V}) + \tilde{B}_2(\mathbf{V}) \le 0, \quad \forall k, \\
& \mathrm{C9}: \mathbf{V} \succeq \mathbf{0},
\end{aligned} \tag{3.19}
$$

where $\mu \to 0$ denotes the penalty factor. The following Theorem 2 reveals the equivalence of the original problem formulation (3.14) and the problem formulation (3.19) based on the penalty method.

Theorem 2. We suppose $\mathbf{V}_s$ is the optimal solution for the problem (3.19) and $\mathbf{V}^\star$ denotes the optimal solution for the problem (3.14), respectively. When the penalty factor is small enough, i.e., $\mu \to 0$, the limit point $\bar{\mathbf{V}} \in \{\mathbf{V}_s\}$ would equal to the $\mathbf{V}^*$.

[4]The SDR proposed in Subproblem 1 may not be available for Subproblem 2 since [74] found that the final answer based on the SDR-SCA method is hard to guarantee SINR constraint, i.e., C2. Accordingly, they propose novel penalty-based algorithms with better performance and convergence guarantees. This is the reason that we use penalty-based algorithms in this thesis.

Proof. Please refer to Appendix B for a proof of Theorem 2. ■

Algorithm 2 Penalty-Based SCA Algorithm

1: Set iteration index $j = 1$
2: Replace $\mathbf{\Phi}$ by $\mathbf{V}$ via (3.12) with $N+1$ random phases
3: Relax the rank-one constraint via Penalty function
4: **repeat**
5: Solve relaxed version problem (3.21) with given $\mathbf{V}^{(j)}$ to update $\mathbf{V}^{(j+1)}$
6: Set $j = j+1$ and update the optimization variables
7: **until** convergence
8: Under $\mathbf{V}^\star = \mathbf{V}^{(j)}$, obtain the $\tilde{\mathbf{v}}^\star$ via EVD decomposition
9: Obtain $\mathbf{\Phi}^\star = \mathrm{Diag}(\mathbf{v}^\star)$

Algorithm 3 The Alternating Optimization Algorithm

1: Assume convergence tolerance ϵ and iteration index $t = 1$
2: Initialize $\mathbf{\Phi}^{(1)}$ to feasible values
3: **repeat**
4: Under the given $\mathbf{\Phi} = \mathbf{\Phi}^{(t)}$, solve problem (3.2) via **Algorithm 1** and store the optimal solution $\{\rho_k^{(t)}, \mathbf{W}_k^{(t)}, \mathbf{W}_{\mathrm{E}}^{(t)}\}$
5: Under the given $\{\rho_k, \mathbf{W}_k, \mathbf{W}_{\mathrm{E}}\} = \{\rho_k^{(t)}, \mathbf{W}_k^{(t)}, \mathbf{W}_{\mathrm{E}}^{(t)}\}$, solve problem (3.11) via **Algorithm 2** and store the optimal solution $\mathbf{\Phi}^{(t+1)}$
6: Update $t = t+1$
7: **until** problem (3.1) converges or $\tau^{(t+1)} - \tau^{(t)} \leq \epsilon$
8: Obtain the solution by $\{\rho_k^\star, \mathbf{W}_k^\star, \mathbf{W}_{\mathrm{E}}\}^\star = \{\rho_k^{(t)}, \mathbf{W}_k^{(t)}, \mathbf{W}_{\mathrm{E}}^{(t)}\}$ and $\mathbf{\Phi}^\star = \mathbf{\Phi}^{(t)}$

According to Theorem 2, the optimal solution of (3.19) is the rank-one solution when penalty factor μ is small. However, the objective function in (3.19) is in the difference of convex form. Then, we can adopt the proposed method SCA to obtain a stationary point. By utilizing the first-order Taylor approximation during each iteration, it is possible to determine the lower bound of $\|\mathbf{V}\|^2$, as follows

$$C(\mathbf{V}) = \|\mathbf{V}\|^2 \geq C(\mathbf{V}^{(t)}) + \mathrm{Tr}\left(\nabla_{\mathbf{V}}^H C(\mathbf{V}^{(t)})(\mathbf{V} - \mathbf{V}^{(t)})\right), \tag{3.20}$$

where the superscript (t) denotes the t-th iteration. Thereby, the problem (3.19) is given

by

$$
\begin{aligned}
\underset{\mathbf{V}}{\text{minimize}} \quad & \frac{1}{\mu}\left(\|\mathbf{V}\|_* - C(\mathbf{V}^{(t)}) - \mathrm{Tr}\left(\nabla_{\mathbf{V}}^H C(\mathbf{V}^{(t)})(\mathbf{V}-\mathbf{V}^{(t)})\right)\right) \\
\text{subject to} \quad & \mathrm{C2}: \frac{\mathrm{Tr}(\mathbf{M}_k\mathbf{W}_k)}{\sum_{i\in\mathcal{K}\setminus\{k\}}\mathrm{Tr}(\mathbf{M}_k\mathbf{W}_i)+\frac{\sigma_{\mathbf{s}}^2}{\rho_k}} \geq \Gamma_{k,\mathrm{req}}, \quad \forall k, \\
& \mathrm{C3}: \textstyle\sum_{i\in\mathcal{K}}\mathrm{Tr}(\mathbf{M}_k\mathbf{W}_i) + \mathrm{Tr}\ (\mathbf{M}_k\mathbf{W}_{\mathrm{E}}) \geq \frac{P_{k,\mathrm{req}}}{\eta(1-\rho_k)}, \\
& \mathrm{C4}: \mathrm{Diag}(\mathbf{V}) = \mathbf{1}_{N+1}, \\
& \mathrm{C6}: \tau_k - A_2(\mathbf{V}) + \tilde{B}_2(\mathbf{V}) \leq 0, \quad \forall k, \\
& \mathrm{C9}: \mathbf{V} \succeq \mathbf{0}.
\end{aligned}
\tag{3.21}
$$

Obviously, problem (3.21) is jointly convex optimization problem with respect to $\mathbf{V}$. So far, the current convex pprogramme tools like CVX can successfully solve it. Next, we can adpot EVD decomposition to recover $\tilde{\mathbf{v}}$ and reconstruct the value of $\mathbf{\Phi}$. The proposed algorithm summarized in **Algorithm 2**, whose results can guaranteed to convergence due to monotonically non-increasing objective function in (3.20) [76]. The overall AO algorithm is summarized in **Algorithm 3**.

Chapter 4

Simulation Results

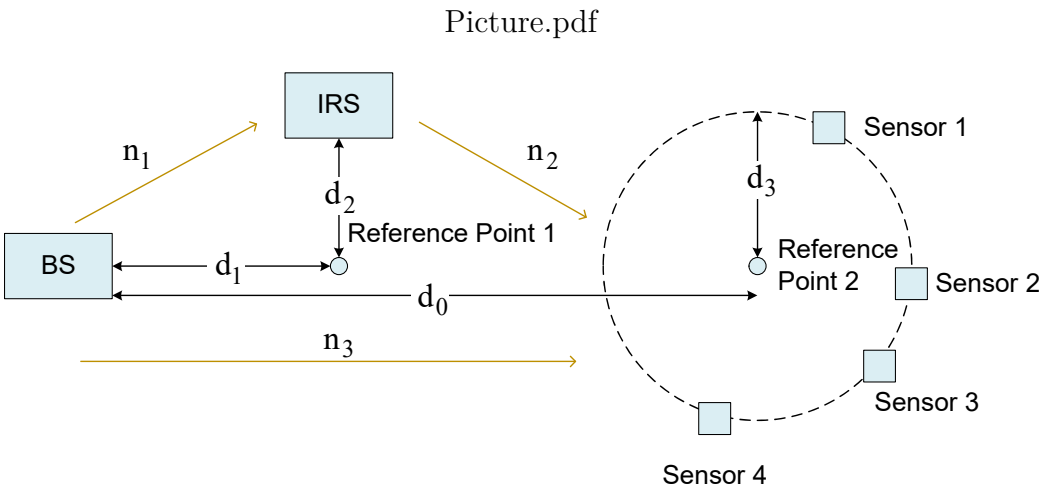

Figure 4.1: Simulation setup.

In this chapter, we evaluate the numerical results of the proposed resource allocation algorithm based on the IRS-assisted network. As shown in Figure 4.1, we assume this system contains $K = 4$ sensors and a single IRS allocated between the BS and sensors. The distance between BS and reference point 1 as well as the distance between the BS and reference point 2, are denoted by $d_1 = 15$ m and $d_0 = 60$ m, respectively. Between IRS and reference point 1, there is a vertical distance of $d_2 = 2$ m. On a circle with a radius of $d_3 = 4$ m from reference point 2, the four sensors are placed at random. In addition, the same channel fading model as in [74] is adopted in this simulation setup[4]. In particular,

[4] The channel vector for the BS-IRS path, e.g. $\mathbf{G}$, and IRS-sensors path, e.g. $\mathbf{h}_{r,k}$, follow the equation (39) in [74] including both large-scale fading and small-scale fading effect. The direct link $\mathbf{h}_{d,k}$ is modeled as Rayleigh fading channel due to the presence of obstacles between the direct links.

n_1, n_2 and n_3 represent the path-loss exponent for the BS-IRS link, the IRS-sensors link, and the BS-sensors link, respectively. Other related simulation parameters for simulation setup are shown in Table 4.1.

Table 4.1: System Parameters

Channel vectors	[74]
Wavelength	$\lambda_c = 0.083$ m
Carrier center frequency	$f_c = 3.6$ GHz
Rician factors	$K_r = 3.4$ dB
Target SINR	$\Gamma_{k,\text{req}} = 9$ dB
Noise power	$\sigma_s = -85$ dBm
Penalty factor	$\mu = 8 \times 10^{-4}$
SCA convergence tolerance	$\epsilon = 10^{-4}$
the BS antenna gains	$G = 1$ dBi
Energy harvesting conversion efficiency	$\eta_k = 0.6$
Target harvested power	$P_{k,\text{req}} = 0.03$ Watt
Path loss exponents for considered paths	$n_1 = 2$, $n_2 = 3$, $n_3 = 5$

4.1 Average Minimum Individual Data Rate versus Maximum Transmit Power

In this section, we simulate the average minimum individual data rate versus the maximum transmit power allowance of the BS for the different number of transmit antennas. Firstly, Figure 4.2 shows that the average minimum individual data rate rises monotonically as the total transmit power increases. This is attributable to an increase in the SINR of each sensor. In other words, the individual data rate is increased by introducing more transmit power to raise the SINR in the framework of the proposed algorithms. Secondly, Figure 4.2 also shows a considerable performance gain by providing more transmit antennas. This comes from the fact that beamforming can effectively exploit the extra degrees of freedom (DoF) provided by IRS, and therefore a remarkable gain happens with deploying additional number of transmit antennas. In consequence, the deployment of

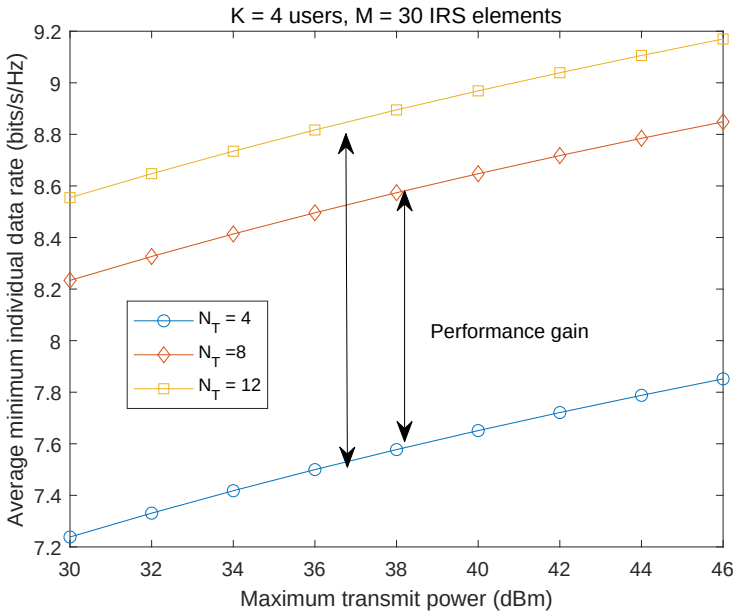

Figure 4.2: Average minimum individual data rate versus maximum transmit power of the BS. The double-sided arrows highlight the performance gain by the increase in the number of transmitting antennas.

the IRS is a driving force to the considerable performance gain, where IRS establishes a more favorable propagation environment for each sensor.

4.2 Average Minimum Individual Data Rate versus Number of Reflecting Elements

Figure 4.3 illustrates the average minimum individual data rate versus the number of reflecting elements at the IRS for different numbers of transmitting antennas. We assume that the value of the maximum transmit power is 30 dBm. It can be observed that the average minimum individual data rate for each sensor increased as long as deploying more reflecting elements at the IRS. This is because the extra reflecting elements can reflect more power from the BS and extends the signal coverage range, which attributes to the higher data rate of the IRS-SWIPT system. Thereby, this observation result validates the considerable advantages of IRS in overcoming the limited coverage problem due to the penetration loss in mmWave frequencies. Secondly, the schemes with $N_{\mathrm{T}} = 12$ or $N_{\mathrm{T}} = 8$ outperform the baseline scheme with $N_{\mathrm{T}} = 4$ over the entire range of reflecting elements,

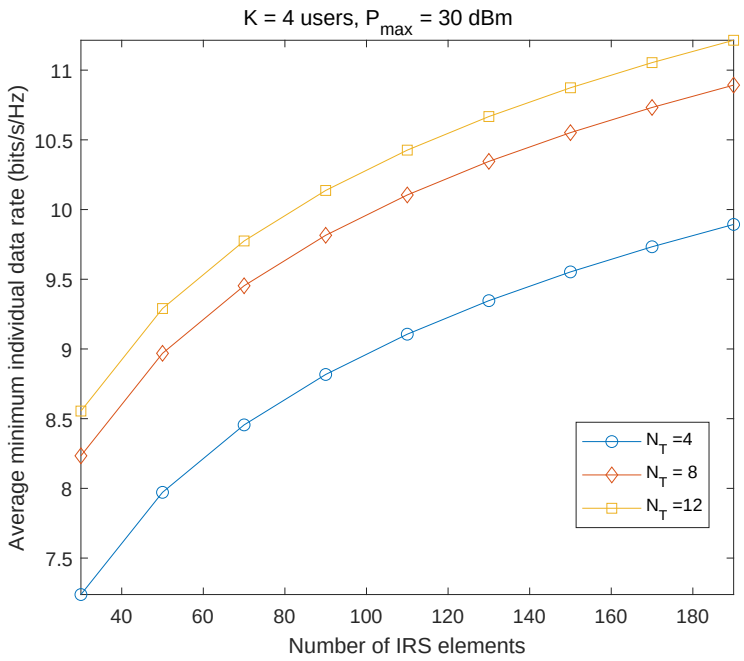

Figure 4.3: Average minimum individual data rate versus the number of reflecting elements at the IRS.

which indicates that the IRS can help the MISO system fully exploit spatial DoF. This result confirms that IRS is available to further improve system performance for the links with extra transmit antennas.

Chapter 5

Conclusion

5.1 Summary of Results

In this thesis, we incorporated IRS in the SWIPT-MISO system to ensure a fair data rate for each sensor by deploying the proposed resource allocation scheme. The simulation results confirm the performance gain achieved by the proposed optimization algorithms. In particular, the extra number of reflecting elements of IRS can significantly improve the minimum individual data rate. In addition, the utilization of IRS proved to be favorable in helping the SWIPT-MISO system to exploit spatial DoF and then save transmit power.

5.2 Future Work

Although this thesis presents the model of IRS-assisted SWIPT communication system with excellent system performance, this model can be further modified to further complicated communication system. Therefore, future work can extend to the design by considering the following two directions. First, this thesis only considers a single IRS in system design. Then, future resource allocation can focus on the system performance by deploying two IRSs or even more. For example, future works could compare the performance gain achieved by multiple IRSs with the gain achieved by additional number of reflecting elements in a single IRS. Second, IRS is a passive device, however, it still needs to consume a small amount of energy. Thus, the future research direction can focus on partially reflective elements to transmit information and partially elements to act as the EH receivers.

Appendix A

We would prove the tightness of SDR and we recast the problem in (3.9) as following presentation

$$
\begin{aligned}
&\underset{\tau_k,\rho_k,\mathbf{W}_k,\mathbf{W}_{\mathrm{E}}}{\text{maximize}} \quad \tau_k \\
&\text{subject to} \quad \mathrm{C1}: \textstyle\sum_{k\in\mathcal{K}} \mathrm{Tr}\left(\mathbf{W}_k\right) + \mathrm{Tr}\left(\mathbf{W}_{\mathrm{E}}\right) \le P_{\max}, \\
&\qquad \mathrm{C2}: \tfrac{\mathrm{Tr}(\mathbf{H}_k\mathbf{W}_k)}{\Gamma_{k,\mathrm{req}}} - \textstyle\sum_{i\in\mathcal{K}\setminus\{k\}} \mathrm{Tr}\left(\mathbf{H}_k\mathbf{W}_i\right) \ge \tfrac{\sigma_s^S}{\rho_k}, \quad \forall k, \\
&\qquad \mathrm{C3}: \textstyle\sum_{i\in\mathcal{K}} \mathrm{Tr}(\mathbf{H}_k\mathbf{W}_i) + \mathrm{Tr}\ \left(\mathbf{H}_k\mathbf{W}_{\mathrm{E}}\right) \ge \tfrac{P_{k,\mathrm{req}}}{\eta(1-\rho_k)}, \\
&\qquad \mathrm{C5}: 0 \le \rho_k \le 1, \quad \forall k, \\
&\qquad \mathrm{C6}: \log_2\left(\eta_k + \tfrac{\sigma_{\mathbf{s}}^2}{\rho_k}\right) - \textstyle\sum_{k\in\mathcal{K}} \mathrm{Tr}\left(\mathbf{W}_k \nabla^H_{\mathbf{W}_k} B_1\right) - \mathrm{Tr}\left(\rho_k \nabla^H_{\rho_k} B_1\right), \quad \forall k, \\
&\qquad \mathrm{C8}: \mathbf{W}_k \succeq \mathbf{0}, \quad \forall k.
\end{aligned}
\tag{A.1}
$$

In order to simplify the expression of (A.1), we would restate this problem in its epigraph form to facilitate the following presentation

$$
\begin{aligned}
&\underset{\tau_k,\rho_k,\mathbf{W}_k,\mathbf{W}_{\mathrm{E}}}{\text{maximize}} \quad \tau_k \\
&\text{subject to} \quad \mathrm{C1}: \textstyle\sum_{k\in\mathcal{K}} \mathrm{Tr}\left(\mathbf{W}_k\right) + \mathrm{Tr}\left(\mathbf{W}_{\mathrm{E}}\right) - P_{\max} \le 0, \\
&\qquad \mathrm{C2}: \tfrac{\sigma_s^S}{\rho_k} - \tfrac{\mathrm{Tr}(\mathbf{H}_k\mathbf{W}_k)}{\Gamma_{k,\mathrm{req}}} + \textstyle\sum_{i\in\mathcal{K}\setminus\{k\}} \mathrm{Tr}\left(\mathbf{H}_k\mathbf{W}_i\right) \le 0, \quad \forall k, \\
&\qquad \mathrm{C3}: \tfrac{P_{k,\mathrm{req}}}{\eta(1-\rho_k)} - \textstyle\sum_{i\in\mathcal{K}} \mathrm{Tr}(\mathbf{H}_k\mathbf{W}_i) - \mathrm{Tr}\ \left(\mathbf{H}_k\mathbf{W}_{\mathrm{E}}\right) \le 0, \\
&\qquad \mathrm{C5}: 0 \le \rho_k \le 1, \quad \forall k, \\
&\qquad \mathrm{C6}: \tau_k - \log_2\left(\eta_k + \tfrac{\sigma_{\mathbf{s}}^2}{\rho_k}\right) + \textstyle\sum_{k\in\mathcal{K}} \mathrm{Tr}\left(\mathbf{W}_k \nabla^H_{\mathbf{W}_k} B_1\right) + \mathrm{Tr}\left(\rho_k \nabla^H_{\rho_k} B_1\right) \le 0, \quad \forall k, \\
&\qquad \mathrm{C8}: -\mathbf{W}_k \preceq \mathbf{0}, \quad \forall k, \\
&\qquad \mathrm{C10}: \eta_k - \mathrm{Tr}(\mathbf{H}_k\mathbf{W}_k) - \textstyle\sum_{i\in\mathcal{K}\setminus\{k\}} \mathrm{Tr}(\mathbf{H}_k\mathbf{W}_i) \ge 0, \quad \forall k,
\end{aligned}
\tag{A.2}
$$

where η_k is the auxiliary variable. Without the rank one constraint shown in C7, this relaxed problem is a typical convex problem and satisfies the Slater's constraint qualification. According to [76], the optimal solution would satisfy the Karush-Kuhn-Tucker

(KKT) conditions under the condition of strong duality. The Lagrangian function of (A.1) with respect to optimization variable $\mathbf{W}_k$ is given by

$$\begin{aligned}\mathcal{L} =&\tau - \sum_{k\in\mathcal{K}} \mathrm{Tr}(\boldsymbol{\Upsilon}_k \mathbf{W}_k) \\ &+ \nu \left(\sum_{k\in\mathcal{K}} \mathrm{Tr}\left(\mathbf{W}_k\right) + \mathrm{Tr}\left(\mathbf{W}_{\mathrm{E}}\right) - P_{\max} \right) \\ &+ \sum_{k\in\mathcal{K}} \psi_k \left(\frac{\sigma_s^S}{\rho_k} - \frac{\mathrm{Tr}\left(\mathbf{H}_k \mathbf{W}_k\right)}{\Gamma_{k,\mathrm{req}}} + \sum_{i\in\mathcal{K}\setminus\{k\}} \mathrm{Tr}\left(\mathbf{H}_k \mathbf{W}_i\right) \right) \\ &+ \sum_{k\in\mathcal{K}} \chi_k \left(\frac{P_{k,\mathrm{req}}}{\eta(1-\rho_k)} - \sum_{i\in\mathcal{K}} \mathrm{Tr}(\mathbf{H}_k \mathbf{W}_i) - \mathrm{Tr}\ \left(\mathbf{H}_k \mathbf{W}_{\mathrm{E}}\right) \right) \\ &+ \sum_{k\in\mathcal{K}} \gamma_k \left(\tau_k - \log_2\left(\eta_k + \frac{\sigma_{\mathbf{s}}^2}{\rho_k}\right) + \sum_{k\in\mathcal{K}} \mathrm{Tr}\left(\mathbf{W}_k \nabla_{\mathbf{W}_k}^H B_1\right) + \mathrm{Tr}\left(\rho_k \nabla_{\rho_k}^H B_1\right) \right) \\ &+ \sum_{k\in\mathcal{K}} \lambda_k \left(\eta_k - \mathrm{Tr}(\mathbf{H}_k \mathbf{W}_k) - \sum_{i\in\mathcal{K}\setminus\{k\}} \mathrm{Tr}(\mathbf{H}_k \mathbf{W}_i) \right),\end{aligned} \tag{A.3}$$

where $\boldsymbol{\Upsilon}_k, \nu, \psi_k, \chi_k, \gamma_k$, and λ_k refer to Lagrange multipliers corresponding to constraints C8, C1, C2, C3, C6, C10, respectively. Next, KKT conditions for the problem in (A.1) based on optimal $\mathbf{W}_k$ can be represented by

$$\begin{aligned}&\mathrm{K1}: \boldsymbol{\Upsilon}_k^\star \mathbf{W}_k^\star = \mathbf{0}, \\ &\mathrm{K2}: \boldsymbol{\Upsilon}_k \succeq \mathbf{0}, \nu_k^\star \geq 0, \psi_k^\star \geq 0, \chi_k^\star \geq 0, \gamma_k^\star \geq 0, \lambda_k^\star \geq 0, \\ &\mathrm{K3}: \nabla_{\mathbf{W}_k} \mathcal{L}(\mathbf{W}_k^\star) = \mathbf{0}, \nabla_{\mathbf{W}_{\mathrm{E}}} \mathcal{L}(\mathbf{W}_{\mathrm{E}}^\star) = \mathbf{0},\end{aligned} \tag{A.4}$$

where $\boldsymbol{\Upsilon}_k, \nu_k^\star, \psi_k^\star, \chi_k^\star, \gamma_k^\star$, and $\lambda_k^\star$ represent the optimal Lagrange multipliers for (A.1). KKT condition K1 is the complementary slackness condition, condition K2 is the dual constraints, and conditions K3 are the gradient of Lagrangian with respect to optimization variables vanishing.

To further process problems, we could recast the equation (A.3) in a more concise representation as follows

$$\mathcal{L} = \mathrm{Tr}(\mathbf{D}_k^\star \mathbf{W}_k) + \mathrm{Tr}(\mathbf{E}_k^\star \mathbf{W}_{\mathrm{E}}) + F_k^\star + \Delta, \tag{A.5}$$

where $\mathbf{D}_k^\star$, $\mathbf{E}_k^\star$, and $\mathbf{F}_k^\star$ contains the coefficient terms associated with $\mathbf{W}_k^\star$, $\mathbf{E}_{\mathrm{E}}^\star$ and all terms related to ρ_k, respectively. Δ denoting all terms that are not relevant with optimization

variables. The expression for $\mathbf{D}_k^\star$, $\mathbf{E}_k^\star$ and $\mathbf{F}_k^\star$ are given by

$$\begin{aligned}\mathbf{D}_k^\star =& -\boldsymbol{\Upsilon}_k^\star \mathbf{I}_{N_\mathrm{T}} + \nu_k^\star \mathbf{I}_{N_\mathrm{T}} - \frac{\psi_k^\star}{\Gamma_{k,\mathrm{req}}}\mathbf{H}_k + \sum_{i\in\mathcal{K}} \psi_i^\star \mathbf{H}_i - \psi_k^\star \mathbf{H}_k \\ & - \sum_{i\in\mathcal{K}} \chi_i^\star \mathbf{H}_i + \mathrm{Tr}(\gamma_k^\star \nabla_{\mathbf{W}_k}^H B_1(\mathbf{W}^{(t)}) + \sum_{i\in\mathcal{K}} \lambda_i^\star \mathbf{H}_i \\ =& (-\boldsymbol{\Upsilon}_k^\star + \nu_k^\star)\mathbf{I}_{N_\mathrm{T}} - \left(\frac{\psi_k^\star}{\Gamma_{k,\mathrm{req}}} + \psi_k^\star\right)\mathbf{H}_k + \mathrm{Tr}(\gamma_k^\star \nabla_{\mathbf{W}_k}^H B_1(\mathbf{W}^{(t)})) \\ & + \sum_{i\in\mathcal{K}} (\psi_i^\star - \chi_i^\star + \lambda_i^\star)\mathbf{H}_i,\end{aligned} \tag{A.6}$$

$$\mathbf{E}_k^\star = -\sum_{k\in\mathcal{K}} \chi_k^\star \mathbf{H}_k + \nu_k^\star \mathbf{I}_{N_\mathrm{T}}, \tag{A.7}$$

$$\mathbf{F}_k^\star = \sum_{k\in\mathcal{K}} \left(-\gamma_k^\star \log_2\left(\eta_k + \frac{\sigma_s^2}{\rho_k}\right) + \psi_k^\star \frac{\sigma_s^2}{\rho_k} + \chi_k^\star \frac{P_{k,\mathrm{req}}}{\eta(1-\rho_k)}\right). \tag{A.8}$$

To further focus on KKT condition K3, i.e., $\nabla_{\mathbf{W}_k}\mathcal{L}(\mathbf{W}_k^\star) = \mathbf{0}$, it can be expressed as follows

$$\underbrace{\nu_k^\star \mathbf{I}_{N_\mathrm{T}} + \gamma_k^\star \nabla_{\mathbf{W}_k}^H B_1(\mathbf{W}^{(t)}) - \sum_{i\in\mathcal{K}} (\psi_i^\star - \chi_i^\star + \lambda_i^\star)\mathbf{H}_i}_{\mathbf{M}_k^\star} - \left(\frac{\psi_k^\star}{\Gamma_{k,\mathrm{req}}} + \psi_k^\star\right)\mathbf{H}_k = \boldsymbol{\Upsilon}_k^\star, \tag{A.9}$$

where we define $\mathbf{M}_k$ to simplify the KKT condition K3 as follows

$$\mathbf{M}_k^\star - \left(\frac{\psi_k^\star}{\Gamma_{k,\mathrm{req}}} + \psi_k^\star\right)\mathbf{H}_k^\star = \boldsymbol{\Upsilon}_k^\star. \tag{A.10}$$

The expression of $\mathbf{M}_k^\star$ is given by

$$\mathbf{M}_k^\star = \nu_k^\star \mathbf{I}_{N_\mathrm{T}} + \gamma_k^\star \nabla_{\mathbf{W}_k}^H B_1(\mathbf{W}^{(t)}) - \sum_{i\in\mathcal{K}} (\psi_i^\star - \chi_i^\star + \lambda_i^\star)\mathbf{H}_i. \tag{A.11}$$

In order to better exploit the rank of the matrix $\mathbf{W}_k$, we first focus on matrix $\mathbf{M}_k^\star$ is full rank with $\mathrm{Rank}(\mathbf{M}_k^\star) = N_\mathrm{T}$. Next, we discuss matrix $\mathbf{M}_k^\star$ is not full rank.

1. **Full Rank**: In this case, matrix $\mathbf{M}_k^\star$ is a full rank matrix. Since $\mathrm{Rank}(\mathbf{H}_k^\star) = 1$, the rank relationship of equality (A.9) yields

$$\mathrm{Rank}(\boldsymbol{\Upsilon}_k^\star) = \mathrm{Rank}(\mathbf{M}_k^\star - \mathbf{H}_k^\star). \tag{A.12}$$

Based on the property of rank, where $\mathrm{Rank}(\mathbf{Y}-\mathbf{Z}) \geq \mathrm{Rank}(\mathbf{Y}) - \mathrm{Rank}(\mathbf{Z})$ [81], we could rewrite (A.12) as follows

$$\mathrm{Rank}(\boldsymbol{\Upsilon}_k^\star) \geq \mathrm{Rank}(\mathbf{M}_k^\star) - \mathrm{Rank}(\mathbf{H}_k^\star) = N_\mathrm{T} - 1. \tag{A.13}$$

First, we assume $\text{Rank}(\boldsymbol{\Upsilon}_k^\star) = N_\text{T} - 1$. Considering the complementary slackness condition K1 : $\boldsymbol{\Upsilon}_k^\star \mathbf{W}_k^\star = \mathbf{0}$, the null space of $\boldsymbol{\Upsilon}_k^\star$ is spanned by the eigenvector $\mathbf{x}_k^\star$. Their rank relationship follows

$$\begin{aligned} & \text{Rank}(\boldsymbol{\Upsilon}_k^\star) = N_\text{T} - \text{Rank}(\mathbf{W}_k^\star), \\ \Rightarrow \quad & \text{Rank}(\mathbf{W}_k^\star) = N_\text{T} - (N_\text{T} - 1) = 1. \end{aligned} \tag{A.14}$$

Furthermore, $\mathbf{W}_k^\star$ can be expressed in the form of eigen-decomposition as follows

$$\mathbf{W}_k^\star = \sum_{i=1}^{N_\text{T}} \lambda_i \mathbf{x}_k^\star (\mathbf{x}_k^\star)^H, \tag{A.15}$$

where $\lambda_1 \geq \lambda_2 \geq \cdots \geq \lambda_{N_\text{T}}$ are the maximum eigenvalues. Next, we assume $\text{Rank}(\boldsymbol{\Upsilon}_k^\star) = N_\text{T}$, then $\text{Rank}(\mathbf{W}_k^\star) = 0$, which leads to zero solution $\mathbf{W}_k^\star = 0$.

Thereby, when the matrix $\mathbf{M}_k^\star$ is full rank, the optimal solution $\mathbf{W}_k^\star$ of problem in (3.3) satisfies the rank-one constraint C7.

2. **Not Full Rank**: In this case, matrix $\mathbf{M}_k^\star$ is not a full rank matrix, i.e., $\text{Rank}(\mathbf{M}_k^\star) \leq N_\text{T}$. We define $r = \text{Rank}(\mathbf{M}_k^\star)$. Suppose $\boldsymbol{\Xi}_k^\star = \sum_{i=1}^{N_\text{T}-r} \xi_{k,i}^\star (\xi_{k,i}^\star)^H$ and the linear combinations of vectors $\xi_{k,j}$ span the null space of $\mathbf{M}_k^\star$, which yields to

$$\mathbf{M}_k^\star \boldsymbol{\Xi}_k^\star = \mathbf{0}, \tag{A.16}$$

where $\text{Rank}(\boldsymbol{\Xi}_k^\star) = N_\text{T} - r$. Based on the KKT condition K2, we have

$$\begin{aligned} & \boldsymbol{\Upsilon}_k \succeq \mathbf{0} \Rightarrow \boldsymbol{\Xi}_k^\star \boldsymbol{\Upsilon}_k \geq \mathbf{0} \\ & \boldsymbol{\Xi}_k^\star \left(\mathbf{M}_k^\star - \left(\frac{\psi_k^\star}{\Gamma_{k,\text{req}}} + \psi_k^\star \right) \mathbf{H}_k^\star \right) \geq \mathbf{0} \\ & \underbrace{\boldsymbol{\Xi}_k^\star \mathbf{M}_k^\star}_{\mathbf{0}} - \boldsymbol{\Xi}_k^\star \left(\frac{\psi_k^\star}{\Gamma_{k,\text{req}}} + \psi_k^\star \right) \mathbf{H}_k^\star \geq \mathbf{0} \\ & \Rightarrow \left(\frac{\psi_k^\star}{\Gamma_{k,\text{req}}} + \psi_k^\star \right) \boldsymbol{\Xi}_k^\star \mathbf{H}_k^\star \leq \mathbf{0}. \end{aligned} \tag{A.17}$$

Since $\psi_k^\star > 0$ from the KKT condition K2, the inequality in (A.17) can yield to

$$\boldsymbol{\Xi}_k^\star \mathbf{H}_k^\star = \mathbf{0}. \tag{A.18}$$

To further exploit the equality in (A.18), we have

$$\begin{aligned} \boldsymbol{\Xi}_k^\star \left(\frac{\psi_k^\star}{\Gamma_{k,\text{req}}} + \psi_k^\star \right) \mathbf{H}_k^\star = \mathbf{0} \Rightarrow \boldsymbol{\Xi}_k^\star \left(\mathbf{M}_k^\star - \boldsymbol{\Upsilon}_k^\star \right) = \mathbf{0} \\ \underbrace{\boldsymbol{\Xi}_k^\star \mathbf{M}_k^\star}_{\mathbf{0}} - \boldsymbol{\Xi}_k^\star \boldsymbol{\Upsilon}_k^\star = \mathbf{0} \\ \boldsymbol{\Xi}_k^\star \boldsymbol{\Upsilon}_k^\star = \mathbf{0}. \end{aligned} \tag{A.19}$$

From the (A.19), it is clear that $\boldsymbol{\Xi}_k^\star$ spans $N_\mathrm{T}-r$ dimensions of $\boldsymbol{\Upsilon}_k^\star$. According to the condition K1 that gives $\boldsymbol{\Upsilon}_k^\star \mathbf{W}_k^\star = \mathbf{0}$, $\mathbf{W}_k^\star$ spans the orthogonal dimensions of $\mathbf{Upsilon}_k^\star$. Therefore, we have

$$\mathrm{Rank}(\mathbf{W}_k^\star) \geq \mathrm{Rank}(\boldsymbol{\Xi}_k^\star) = N_\mathrm{T} - r. \tag{A.20}$$

With $\mathrm{Rank}(\mathbf{A}-\mathbf{B}) \geq \mathrm{Rank}(\mathbf{A}) - \mathrm{Rank}(\mathbf{B})$, the rank of $\boldsymbol{\Upsilon}_k^\star$ is given by

$$\begin{aligned} \mathrm{Rank}(\boldsymbol{\Upsilon}_k^\star) &\geq \mathrm{Rank}(\mathbf{M}_k^\star) - \mathrm{Rank}(\mathbf{H}_k^\star) = r-1, \\ &\Rightarrow -\mathrm{Rank}(\boldsymbol{\Upsilon}_k^\star) \leq 1-r. \end{aligned} \tag{A.21}$$

Thereby, we have

$$\begin{aligned} \mathrm{Rank}(\mathbf{W}_k^\star) &= N_\mathrm{T} - \mathrm{Rank}(\boldsymbol{\Upsilon}_k^\star) \\ &\leq N_\mathrm{T} + 1 - r. \end{aligned} \tag{A.22}$$

Based on inequalities (A.20) and (A.22), we have

$$N_\mathrm{T} - r \leq \mathrm{Rank}(\mathbf{W}_k^\star) \leq N_\mathrm{T} + 1 - r, \tag{A.23}$$

where the rank of $\mathbf{W}_k^\star$ has two cases, one is $\mathrm{Rank}(\mathbf{W}_k^\star) = N_\mathrm{T} - r$ and another is $\mathrm{Rank}(\mathbf{W}_k^\star) = N_\mathrm{T} + 1 - r$. When the rank of $\mathbf{W}_k^\star$ satisfy the first situation, we have

$$\boldsymbol{\Xi}_k^\star \boldsymbol{\Upsilon}_k^\star = \mathbf{0}, \mathbf{W}_k^\star \boldsymbol{\Upsilon}_k^\star = \mathbf{0}, \quad \Rightarrow \boldsymbol{\Xi}_k = \mathbf{W}_k^\star, \tag{A.24}$$

which is proved in the expression of (A.19). Due to the equality $\boldsymbol{\Xi}_k^\star \mathbf{H}_k^\star = \mathbf{0}$ in (A.18), $\mathbf{W}_k^\star$ satisfies $\mathbf{W}_k^\star \mathbf{H}_k^\star = \mathbf{0}$. This cannot be the optimal solution to the primal problem, where this solution indicates zero power allocated to any sensor k during the process of beamforming. When the rank of $\mathbf{W}_k^\star$ satisfy the second situation ($\mathrm{Rank}(\mathbf{W}_k^\star) = N_\mathrm{T} + 1 - r$), the rank of $\mathbf{W}_k^\star$ can be rewritten as

$$\begin{aligned} \mathbf{W}_k^\star &= [\boldsymbol{\Xi}_k^\star \quad \omega_k^\star], \\ &= \lambda_{k,\omega}^\star \omega_k^\star (\omega_k^\star)^H + \sum_{i=1}^{N_\mathrm{T}-r} \lambda_{k,\xi} \xi_{k,i}^\star (\xi_{k,i}^\star)^H, \end{aligned} \tag{A.25}$$

which is valid due to $\mathrm{Rank}(\boldsymbol{\Xi}_k^\star) = N_\mathrm{T} - r$ and $\boldsymbol{\Xi}_k^\star \boldsymbol{\Upsilon}_k^\star = \mathbf{0}$. In addition, $\lambda_{k,\omega}^\star$ and $\lambda_{k,\xi}$ represent the scaling factors for corresponding basis vectors, respectively. This optimal solution $\mathbf{W}_k^\star$ can be further written in format with rank-one expression as follows

$$\tilde{\mathbf{W}}_k^\star = \mathbf{W}_k^\star - \sum_{i=1}^{N_\mathrm{T}-r} \lambda_{k,\xi} \xi_{k,i}^\star (\xi_{k,i}^\star)^H = \lambda_{k,\omega}^\star \omega_k^\star (\omega_k^\star)^H. \tag{A.26}$$

At the same time, we have

$$\tilde{\mathbf{W}}_{\mathrm{E}} = \mathbf{W}_{\mathrm{E}}^{\star} + \sum_{i=1}^{N_{\mathrm{T}}-r} \lambda_{k,\xi} \xi_{k,i}^{\star} (\xi_{k,i}^{\star})^{H}. \tag{A.27}$$

If we can prove the rank-one solution $\tilde{\mathbf{W}}_k^{\star}$ equal to the original optimal solution $\mathbf{W}_k^{\star}$, which further indicates the tight rank relaxation. In order to focus on the more precise equation, we keep the interference from energy signal $\mathbf{w}_{\mathrm{E}}$, which is ignored in (2.6). Thereby, the data rate can be recast as follows

$$\begin{aligned}
\hat{R}_k &= \log_2 \left(1 + \frac{\mathrm{Tr}(\mathbf{H}_k \mathbf{W}_k)}{\mathrm{Tr}(\mathbf{H}_k \mathbf{W}_{\mathrm{E}}) + \sum_{i \in \mathcal{K} \setminus \{k\}} \mathrm{Tr}(\mathbf{H}_k \mathbf{W}_i) + \frac{\delta_s^2}{\rho_k}} \right) \\
&= \log_2 \left(\mathrm{Tr}(\mathbf{H}_k \mathbf{W}_k) + \mathrm{Tr}(\mathbf{H}_k \mathbf{W}_{\mathrm{E}}) + \sum_{i \in \mathcal{K} \setminus \{k\}} \mathrm{Tr}(\mathbf{H}_k \mathbf{W}_i) + \frac{\delta_s^2}{\rho_k} \right) \\
&\quad - \log_2 \left(\mathrm{Tr}(\mathbf{H}_k \mathbf{W}_{\mathrm{E}}) + \sum_{i \in \mathcal{K} \setminus \{k\}} \mathrm{Tr}(\mathbf{H}_k \mathbf{W}_i) + \frac{\delta_s^2}{\rho_k} \right).
\end{aligned} \tag{A.28}$$

We follow the same principle as (3.6), the achievable rate can be further expressed as follows

$$\begin{aligned}
\hat{R}_k =& \log_2 \left(\mathrm{Tr}(\mathbf{H}_k \mathbf{W}_k) + \mathrm{Tr}(\mathbf{H}_k \mathbf{W}_{\mathrm{E}}) + \sum_{i \in \mathcal{K} \setminus \{k\}} \mathrm{Tr}(\mathbf{H}_k \mathbf{W}_i) + \frac{\delta_s^2}{\rho_k} \right) \\
&- \sum_{k \in \mathcal{K}} \mathrm{Tr}(\mathbf{W}_k \nabla_{\mathbf{W}_k}^{H} B_1) - \mathrm{Tr}(\mathbf{W}_{\mathrm{E}} \nabla_{\mathbf{W}_{\mathrm{E}}}^{H} B_1),
\end{aligned} \tag{A.29}$$

where

$$\begin{aligned}
\nabla_{\mathbf{W}_k}^{H} B_1 &= \frac{1}{\ln 2} \frac{\mathbf{H}_k}{\mathrm{Tr}(\mathbf{H}_k \mathbf{W}_{\mathrm{E}}) + \sum_{i \in \mathcal{K} \setminus \{k\}} \mathrm{Tr}(\mathbf{H}_k \mathbf{W}_i) + \frac{\delta_s^2}{\rho_k}}, \\
\nabla_{\mathbf{W}_{\mathrm{E}}}^{H} B_1 &= \frac{1}{\ln 2} \frac{\mathbf{H}_k}{\mathrm{Tr}(\mathbf{H}_k \mathbf{W}_{\mathrm{E}}) + \sum_{i \in \mathcal{K} \setminus \{k\}} \mathrm{Tr}(\mathbf{H}_k \mathbf{W}_i) + \frac{\delta_s^2}{\rho_k}}.
\end{aligned} \tag{A.30}$$

In (A.29), some unrelated constant terms are ignored. Hence, the problem formu-

lation of (3.10) can be recast as follows

$$
\begin{aligned}
\underset{\tau_k,\rho_k,\mathbf{W}_k,\mathbf{W}_{\mathrm{E}}}{\text{maximize}} \quad & \tau_k \\
\text{subject to} \quad & \mathrm{C1}: \textstyle\sum_{k\in\mathcal{K}} \mathrm{Tr}\left(\mathbf{W}_k\right) + \mathrm{Tr}\left(\mathbf{W}_{\mathrm{E}}\right) \le P_{\max}, \\
& \mathrm{C2}: \frac{\mathrm{Tr}(\mathbf{H}_k\mathbf{W}_k)}{\mathrm{Tr}(\mathbf{H}_k\mathbf{W}_{\mathrm{E}})+\sum_{i\in\mathcal{K}\setminus\{k\}}\mathrm{Tr}(\mathbf{H}_k\mathbf{W}_i)+\frac{\delta_s^2}{\rho_k}} \ge \Gamma_{k,\mathrm{req}}, \quad \forall k, \\
& \mathrm{C3}: \textstyle\sum_{i\in\mathcal{K}} \mathrm{Tr}(\mathbf{H}_k\mathbf{W}_i) + \mathrm{Tr}\ \left(\mathbf{H}_k\mathbf{W}_{\mathrm{E}}\right) \ge \frac{P_{k,\mathrm{req}}}{\eta(1-\rho_k)}, \\
& \mathrm{C5}: 0 \le \rho_k \le 1, \quad \forall k, \\
& \mathrm{C6}: \tau_k \le \log_2\left(\mathrm{Tr}(\mathbf{H}_k\mathbf{W}_k) + \mathrm{Tr}(\mathbf{H}_k\mathbf{W}_{\mathrm{E}}) + \textstyle\sum_{i\in\mathcal{K}\setminus\{k\}}\mathrm{Tr}(\mathbf{H}_k\mathbf{W}_i) + \frac{\delta_s^2}{\rho_k}\right) \\
& \qquad - \textstyle\sum_{k\in\mathcal{K}} \mathrm{Tr}(\mathbf{W}_k\nabla^H_{\mathbf{W}_k}B_1) - \mathrm{Tr}(\mathbf{W}_{\mathrm{E}}\nabla^H_{\mathbf{W}_{\mathrm{E}}}B_1), \quad \forall k, \\
& \mathrm{C8}: \mathbf{W}_k \succeq \mathbf{0}, \quad \forall k.
\end{aligned}
\tag{A.31}
$$

Since $\mathbf{W}^\star_{\mathrm{E}} + \sum_{k\in\mathcal{K}}\mathbf{W}^\star_k = \tilde{\mathbf{W}}^\star_{\mathrm{E}} + \sum_{k\in\mathcal{K}}\tilde{\mathbf{W}}^\star_k$, the constraints C1, C2 and C3 have the same feasible sets with the solution of $\{\mathbf{W}^\star_{\mathrm{E}}, \mathbf{W}^\star_k\}$ or $\{\tilde{\mathbf{W}}^\star_{\mathrm{E}}, \tilde{\mathbf{W}}^\star_k\}$. The final uncertainty is about constraint C7. Accordingly, we have

$$
\begin{aligned}
\mathrm{C7}: & \Delta' - \sum_{k\in\mathcal{K}} \mathrm{Tr}(\mathbf{W}_k\nabla^H_{\mathbf{W}_k}B_1) - \mathrm{Tr}(\mathbf{W}_{\mathrm{E}}\nabla^H_{\mathbf{W}_{\mathrm{E}}}B_1) \\
& = \Delta' - \frac{2\mathbf{H}_k}{\ln 2\left(\mathrm{Tr}(\mathbf{H}_k\mathbf{W}_{\mathrm{E}}) + \sum_{i\in\mathcal{K}\setminus\{k\}}\mathrm{Tr}(\mathbf{H}_k\mathbf{W}_i) + \frac{\delta_s^2}{\rho_k}\right)}, \\
& = \Delta' - \frac{2\mathbf{H}_k}{\ln 2\left(\mathrm{Tr}\left[\left(\mathbf{W}_{\mathrm{E}} + \sum_{i\in\mathcal{K}\setminus\{k\}}\mathbf{W}_i\right)\mathbf{H}_k\right] + \frac{\delta_s^2}{\rho_k}\right)},
\end{aligned}
\tag{A.32}
$$

where Δ' denotes some irrelative terms. When we put $\{\tilde{\mathbf{W}}^\star_{\mathrm{E}}, \tilde{\mathbf{W}}^\star_k\}$ into equation (A.32), we have

$$
\begin{aligned}
& \left(\tilde{\mathbf{W}}_{\mathrm{E}} + \sum_{i\in\mathcal{K}\setminus\{k\}}\tilde{\mathbf{W}}_i\right)\mathbf{H}_k \\
& = \left(\mathbf{W}^\star_{\mathrm{E}} + \sum_{i=1}^{N_{\mathrm{T}}-r}\lambda_{k,\xi}\xi^\star_{k,i}(\xi^\star_{k,i})^H\right)\mathbf{H}_k + \left(\sum_{i\in\mathcal{K}\setminus\{k\}}\left(\mathbf{W}^\star_k - \sum_{i=1}^{N_{\mathrm{T}}-r}\lambda_{k,\xi}\xi^\star_{k,i}(\xi^\star_{k,i})^H\right)\right)\mathbf{H}_k \\
& \overset{(a)}{=} \left(\mathbf{W}^\star_{\mathrm{E}} + \sum_{i\in\mathcal{K}\setminus\{k\}}\mathbf{W}^\star_k\right)\mathbf{H}_k,
\end{aligned}
\tag{A.33}
$$

where (a) represent the proved result in (A.18), i.e., $\mathbf{\Xi}^\star_k\mathbf{H}^\star_k = \mathbf{0}$, and some unrelated terms are ignored in this formula presentation. It is shown that the values of $\{\tilde{\mathbf{W}}^\star_{\mathrm{E}}, \tilde{\mathbf{W}}^\star_k\}$ and $\{\mathbf{W}^\star_{\mathrm{E}}, \mathbf{W}^\star_k\}$ are equal in this optimization problem.

As a result, the constraint relaxation is tight. When $\mathbf{B}_k^\star$ is full rank, then the optimal solution $\mathbf{W}_k^\star$ satisfy the rank-one constraint. When $\mathbf{B}_k^\star$ is not full rank, then the optimal solution $\tilde{\mathbf{W}}_k^\star$ with $\text{Rank}(\tilde{\mathbf{W}}_k^\star) = 1$ is equivalent to the optimal solution $\mathbf{W}_k^\star$.

Appendix B

As mentioned before, we assume that $\mathbf{V}^\star$ and $\mathbf{V}_s$ denote optimal solutions of (3.14) and (3.19), respectively. To further verify the condition that $\mathbf{V}^\star$ is equivalent to $\mathbf{V}_s$, we define the objective function in (3.14) as $f_1(\mathbf{V})$ and the objective function in (3.19) as $f_2(\mathbf{V},\mu)$. Since $\mathbf{V}^\star$ satisfy the rank-one constraint, then we could have $\|\mathbf{V}^\star\|_* - \|\mathbf{V}^\star\|_2 \leq 0$. Besides, in terms of all $\mathbf{V}$ that satisfies $\|\mathbf{V}_*\| - \|\mathbf{V}\|_2 = 0$, the optimal solutions $\mathbf{V}^\star$ of the problem in (3.14) yields to $f_1(\mathbf{V}^\star) \leq f_1(\mathbf{V})$. On the other hand, the optimal solution $\mathbf{V}_s$ of the problem in (3.19) yields to $f_2(\mathbf{V}_s,\mu_s) \leq f_2(\mathbf{V}^\star,\mu_s)$. Accordingly, we have

$$\begin{aligned} & f_2(\mathbf{V}_s,\mu_s) \leq f_2(\mathbf{V}^\star,\mu_s), \\ \Rightarrow\ & f_1(\mathbf{V}_s) + \frac{1}{\mu_s}(\|\mathbf{V}_s\|_* - \|\mathbf{V}_s\|_2) \leq f_1(\mathbf{V}^\star) + \underbrace{\frac{1}{\mu_s}(\|\mathbf{V}^\star\|_* - \|\mathbf{V}^\star\|_2)}_{\mathbf{0}}, \\ \Rightarrow\ & f_1(\mathbf{V}_s) + \frac{1}{\mu_s}(\|\mathbf{V}_s\|_* - \|\mathbf{V}_s\|_2) \leq f_1(\mathbf{V}^\star), \\ & \Rightarrow \|\mathbf{V}_s\|_* - \|\mathbf{V}_s\|_2 \leq \mu_s\left(f_1(\mathbf{V}^\star) - f_1(\mathbf{V}_s)\right). \end{aligned} \tag{B.1}$$

Suppose the feasible solution sets as $\{\mathbf{V}_s\}$ and $\bar{\mathbf{V}}_s$ as the limit point belonging to $\{\mathbf{V}_s\}$, this yields to $\lim_{s\in\mathcal{S}} \mathbf{V}_s = \bar{\mathbf{V}}$, where $\mathcal{S}$ denotes an infinite subsequence. First, we consider taking the limitation,i.e., $s \to \infty$, on both side of problem in (B.1) as follows

$$\begin{aligned} \lim_{s\in\mathcal{S}}(\|\mathbf{V}_s\|_* - \|\mathbf{V}_s\|_2) &\leq \lim_{s\in\mathcal{S}} \mu_s\left(f_1(\mathbf{V}^\star) - f_1(\mathbf{V}_s)\right), \\ \Rightarrow \|\bar{\mathbf{V}}_s\|_* - \|\bar{\mathbf{V}}_s\|_2 &\leq \lim_{s\in\mathcal{S}} \mu_s\left(f_1(\mathbf{V}^\star) - f_1(\mathbf{V}_s)\right). \end{aligned} \tag{B.2}$$

When the penalty factor μ_s is sufficiently small, such as $\mu_s \to 0$, the value on the right-hand side of the inequality in (B.2) would converge to 0. In other words, $\|\bar{\mathbf{V}}_s\|_* - \|\bar{\mathbf{V}}_s\|_2 = 0$ with a small enough penalty factor. As a result, we could conclude that the limit point $\bar{\mathbf{V}}_s$ belongs to the solution of the problem in (3.14), where it satisfies the rank-one constraint. Next, we would prove this value is an optimal solution to the problem in

(3.14) as follows

$$
\begin{aligned}
& f_1(\bar{\mathbf{V}}_s) \leq f_1(\bar{\mathbf{V}}_s) + \lim_{s \in \mathcal{S}} \frac{1}{\mu_s} \left(\|\mathbf{V}_s\|_* - \|\mathbf{V}_s\|_2 \right), \\
& \Rightarrow f_1(\bar{\mathbf{V}}_s) + \lim_{s \in \mathcal{S}} \frac{1}{\mu_s} \left(\|\mathbf{V}_s\|_* - \|\mathbf{V}_s\|_2 \right) \leq f_1(\mathbf{V}^\star), \\
& \Rightarrow f_1(\bar{\mathbf{V}}_s) \leq f_1(\mathbf{V}^\star),
\end{aligned}
\tag{B.3}
$$

where the objective function results with $\bar{\mathbf{V}}_s$ is no larger than the counterpart result with $\mathbf{V}^\star$. Thereby, the optimal solution $\bar{\mathbf{V}}_s$ of the problem in (3.19) is also the optimal solution to the problem in (3.14).

Bibliography

[1] D. W. K. Ng, T. Q. Duong, C. Zhong, and R. Schober, *Wireless information and power transfer: theory and practice*. John Wiley & Sons, 2019.

[2] Z. Popović, E. A. Falkenstein, D. Costinett, and R. Zane, "Low-power far-field wireless powering for wireless sensors," *Proceedings of the IEEE*, vol. 101, no. 6, pp. 1397–1409, 2013.

[3] E. Mihret and G. Haile, "4G, 5G, 6G, 7G and future mobile technologies," *J Comp Sci Info Technol*, vol. 9, no. 2, p. 75, 2021.

[4] N. Bhandari, S. Devra, and K. Singh, "Evolution of cellular network: from 1G to 5G," *International journal of engineering and techniques*, vol. 3, no. 5, pp. 98–105, 2017.

[5] S. Shukla, V. Khare, S. Garg, and P. Sharma, "Comparative study of 1G, 2G, 3G and 4G," *J. Eng. Comput. Appl. Sci*, vol. 2, no. 4, pp. 55–63, 2013.

[6] T. Seymour, A. Shaheen *et al.*, "History of wireless communication," *Review of Business Information Systems (RBIS)*, vol. 15, no. 2, pp. 37–42, 2011.

[7] L. J. Vora, "Evolution of mobile generation technology: 1G to 5G and review of upcoming wireless technology 5G," *International journal of modern trends in engineering and research*, vol. 2, no. 10, pp. 281–290, 2015.

[8] J. A. del Peral-Rosado, R. Raulefs, J. A. López-Salcedo, and G. Seco-Granados, "Survey of cellular mobile radio localization methods: From 1G to 5G," *IEEE Communications Surveys Tutorials*, vol. 20, no. 2, pp. 1124–1148, 2018.

[9] A. A. Salih, S. Zeebaree, A. S. Abdulraheem, R. R. Zebari, M. Sadeeq, and O. M.

Ahmed, "Evolution of mobile wireless communication to 5G revolution," *Technology Reports of Kansai University*, vol. 62, no. 5, pp. 2139–2151, 2020.

[10] A. U. Gawas, "An overview on evolution of mobile wireless communication networks: 1G-6G," *International Journal on Recent and Innovation Trends in Computing and Communication*, vol. 3, no. 5, pp. 3130–3133, 2015.

[11] Q. Wu, G. Y. Li, W. Chen, D. W. K. Ng, and R. Schober, "An overview of sustainable green 5G networks," *IEEE Wireless Commun.*, vol. 24, no. 4, pp. 72–80, 2017.

[12] Q. Wu, J. Xu, Y. Zeng, D. W. K. Ng, N. Al-Dhahir, R. Schober, and A. L. Swindlehurst, "A comprehensive overview on 5G-and-beyond networks with UAVs: From communications to sensing and intelligence," *IEEE Journal on Selected Areas in Communications*, 2021.

[13] V. W. Wong, R. Schober, D. W. K. Ng, and L.-C. Wang, *Key technologies for 5G wireless systems*. Cambridge university press, 2017.

[14] W. Xu, Z. Yang, D. W. K. Ng, M. Levorato, Y. C. Eldar *et al.*, "Edge learning for b5g networks with distributed signal processing: Semantic communication, edge computing, and wireless sensing," *arXiv preprint arXiv:2206.00422*, 2022.

[15] M. Breiling, D. W. K. Ng, C. Rohde, F. Burkhardt, and R. Schober, "Sudas: mmWave relaying for 5G outdoor-to-indoor communications," *Institution of Engineering and Technology*, 2016.

[16] Q. Wu, G. Y. Li, W. Chen, D. W. K. Ng, and R. Schober, "An overview of sustainable green 5G networks," *IEEE Wireless Communications*, vol. 24, no. 4, pp. 72–80, 2017.

[17] S. Gong, X. Lu, D. T. Hoang, D. Niyato, L. Shu, D. I. Kim, and Y.-C. Liang, "Toward smart wireless communications via intelligent reflecting surfaces: A contemporary survey," *IEEE Communications Surveys & Tutorials*, vol. 22, no. 4, pp. 2283–2314, 2020.

[18] G. Chittimoju and U. D. Yalavarthi, "A comprehensive review on millimeter waves applications and antennas," in *Journal of Physics: Conference Series*, vol. 1804, no. 1. IOP Publishing, 2021, p. 012205.

[19] X. Yu, V. Jamali, D. Xu, D. W. K. Ng, and R. Schober, "Smart and reconfigurable wireless communications: From IRS modeling to algorithm design," *IEEE Wireless Commun.*, 2021.

[20] Wu, Qingqing and Zhang, Rui, "Towards smart and reconfigurable environment: Intelligent reflecting surface aided wireless network," *IEEE Communications Magazine*, vol. 58, no. 1, pp. 106–112, 2020.

[21] K. Guo, C. Wang, Z. Li, D. W. K. Ng, and K.-K. Wong, "Multiple UAV-borne IRS-aided millimeter wave multicast communications: A joint optimization framework," *IEEE Communications Letters*, vol. 25, no. 11, pp. 3674–3678, 2021.

[22] S. Hu, C. Liu, Z. Wei, Y. Cai, D. W. K. Ng, and J. Yuan, "Beamforming design for intelligent reflecting surface-enhanced symbiotic radio systems," *arXiv preprint arXiv:2110.10316*, 2021.

[23] W. Yan, X. Yuan, and X. Kuai, "Passive beamforming and information transfer via large intelligent surface," *IEEE Wireless Communications Letters*, vol. 9, no. 4, pp. 533–537, 2019.

[24] L. Dai, B. Wang, M. Wang, X. Yang, J. Tan, S. Bi, S. Xu, F. Yang, Z. Chen, M. Di Renzo *et al.*, "Reconfigurable intelligent surface-based wireless communications: Antenna design, prototyping, and experimental results," *IEEE Access*, vol. 8, pp. 45 913–45 923, 2020.

[25] W. Yan, X. Yuan, Z.-Q. He, and X. Kuai, "Passive beamforming and information transfer design for reconfigurable intelligent surfaces aided multiuser MIMO systems," *IEEE Journal on Selected Areas in Communications*, vol. 38, no. 8, pp. 1793–1808, 2020.

[26] Z. Zhang, Q. Sun, J. Zhang, D. W. K. Ng, and B. Ai, "Ergodic capacity of intelligent omni-surface-aided communication systems with phase quantization errors and outdated CSI," *IEEE Systems Journal*, pp. 1–10, 2022.

[27] Y. Cai, Z. Wei, S. Hu, C. Liu, D. W. K. Ng, and J. Yuan, "Resource allocation and 3D trajectory design for power-efficient IRS-assisted UAV-NOMA communications," *IEEE Transactions on Wireless Communications*, 2022.

[28] Y. Teng, M. Liu, F. R. Yu, V. C. Leung, M. Song, and Y. Zhang, "Resource allocation for ultra-dense networks: A survey, some research issues and challenges," *IEEE Communications Surveys & Tutorials*, vol. 21, no. 3, pp. 2134–2168, 2018.

[29] X. Zhu and B. Girod, "Distributed media-aware rate allocation for wireless video streaming," *IEEE Transactions on Circuits and Systems for Video Technology*, vol. 20, no. 11, pp. 1462–1474, 2010.

[30] S. Huaizhou, R. V. Prasad, E. Onur, and I. Niemegeers, "Fairness in wireless networks: Issues, measures and challenges," *IEEE Communications Surveys & Tutorials*, vol. 16, no. 1, pp. 5–24, 2013.

[31] E. Altman, K. Avrachenkov, and A. Garnaev, "Generalized α-fair resource allocation in wireless networks," in *2008 47th IEEE Conference on Decision and Control*. IEEE, 2008, pp. 2414–2419.

[32] C. Guo, M. Sheng, Y. Zhang, and X. Wang, "A Jain's index perspective on α-fairness resource allocation over slow fading channels," *IEEE Communications Letters*, vol. 17, no. 4, pp. 705–708, 2013.

[33] D. Tse and P. Viswanath, *Fundamentals of wireless communication*. Cambridge university press, 2005.

[34] P. Marbach, "Priority service and max-min fairness," in *Proceedings. Twenty-First Annual Joint Conference of the IEEE Computer and Communications Societies*, vol. 1. IEEE, 2002, pp. 266–275.

[35] L. Massoulié and J. Roberts, "Bandwidth sharing: objectives and algorithms," in *IEEE INFOCOM'99. Conference on Computer Communications. Proceedings. Eighteenth Annual Joint Conference of the IEEE Computer and Communications Societies. The Future is Now (Cat. No. 99CH36320)*, vol. 3. IEEE, 1999, pp. 1395–1403.

[36] T. Bonald, L. Massoulié, A. Proutiere, and J. Virtamo, "A queueing analysis of max-min fairness, proportional fairness and balanced fairness," *Queueing systems*, vol. 53, no. 1, pp. 65–84, 2006.

[37] Z. Wei, X. Yu, D. W. K. Ng, and R. Schober, "Resource allocation for simultaneous wireless information and power transfer systems: A tutorial overview," *Proceedings of the IEEE*, 2021.

[38] Z. Zhang, H. Pang, A. Georgiadis, and C. Cecati, "Wireless power transfer—an overview," *IEEE Transactions on Industrial Electronics*, vol. 66, no. 2, pp. 1044–1058, 2018.

[39] M. T. Nguyen, C. V. Nguyen, L. H. Truong, A. M. Le, T. V. Quyen, A. Masaracchia, and K. A. Teague, "Electromagnetic field based wpt technologies for uavs: A comprehensive survey," *Electronics*, vol. 9, no. 3, p. 461, 2020.

[40] X. Mou and H. Sun, "Wireless power transfer: Survey and roadmap," in *2015 IEEE 81st Vehicular Technology Conference (VTC Spring)*. IEEE, 2015, pp. 1–5.

[41] E. Bou-Balust, A. P. Hu, and E. Alarcon, "Scalability analysis of SIMO non-radiative resonant wireless power transfer systems based on circuit models," *IEEE Transactions on Circuits and Systems I: Regular Papers*, vol. 62, no. 10, pp. 2574–2583, 2015.

[42] R. Pudur, V. Hanumante, S. Shukla, and K. Kumar, "Wireless power transmission: A survey," in *International Conference on Recent Advances and Innovations in Engineering (ICRAIE-2014)*. IEEE, 2014, pp. 1–6.

[43] A. Kurs, A. Karalis, R. Moffatt, J. D. Joannopoulos, P. Fisher, and M. Soljacic, "Wireless power transfer via strongly coupled magnetic resonances," *Science*, vol. 317, no. 5834, pp. 83–86, 2007.

[44] T. D. P. Perera, D. N. K. Jayakody, S. K. Sharma, S. Chatzinotas, and J. Li, "Simultaneous wireless information and power transfer (SWIPT): Recent advances and future challenges," *IEEE Communications Surveys & Tutorials*, vol. 20, no. 1, pp. 264–302, 2017.

[45] S. Y. R. Hui, W. Zhong, and C. K. Lee, "A critical review of recent progress in mid-range wireless power transfer," *IEEE Transactions on Power Electronics*, vol. 29, no. 9, pp. 4500–4511, 2013.

[46] A. Mahmood, A. Ismail, Z. Zaman, H. Fakhar, Z. Najam, M. Hasan, and S. Ahmed, "A comparative study of wireless power transmission techniques," *Journal of Basic and Applied Scientific Research*, vol. 4, no. 1, pp. 321–326, 2014.

[47] I. Krikidis, S. Timotheou, S. Nikolaou, G. Zheng, D. W. K. Ng, and R. Schober, "Simultaneous wireless information and power transfer in modern communication systems," *IEEE Communications Magazine*, vol. 52, no. 11, pp. 104–110, 2014.

[48] R. Zhang and C. K. Ho, "MIMO broadcasting for simultaneous wireless information and power transfer," *IEEE Transactions on Wireless Communications*, vol. 12, no. 5, pp. 1989–2001, 2013.

[49] D. W. K. Ng, E. S. Lo, and R. Schober, "Wireless information and power transfer: Energy efficiency optimization in OFDMA systems," *IEEE Transactions on Wireless Communications*, vol. 12, no. 12, pp. 6352–6370, 2013.

[50] C. R. Valenta and G. D. Durgin, "Harvesting wireless power: Survey of energy-harvester conversion efficiency in far-field, wireless power transfer systems," *IEEE Microwave Magazine*, vol. 15, no. 4, pp. 108–120, 2014.

[51] E. Boshkovska, D. W. K. Ng, N. Zlatanov, A. Koelpin, and R. Schober, "Robust resource allocation for MIMO wireless powered communication networks based on a non-linear eh model," *IEEE Transactions on Communications*, vol. 65, no. 5, pp. 1984–1999, 2017.

[52] R. Morsi, V. Jamali, A. Hagelauer, D. W. K. Ng, and R. Schober, "Conditional capacity and transmit signal design for SWIPT systems with multiple nonlinear energy harvesting receivers," *IEEE Transactions on Communications*, vol. 68, no. 1, pp. 582–601, 2019.

[53] Q. Wu, M. Tao, D. W. K. Ng, W. Chen, and R. Schober, "Energy-efficient resource allocation for wireless powered communication networks," *IEEE Transactions on Wireless Communications*, vol. 15, no. 3, pp. 2312–2327, 2015.

[54] H. Ju and R. Zhang, "Throughput maximization in wireless powered communication networks," *IEEE Transactions on Wireless Communications*, vol. 13, no. 1, pp. 418–428, 2013.

[55] C. Boyer and S. Roy, "Backscatter communication and RFID: Coding, energy, and mimo analysis. communications," *IEEE Transactions on*, 2013.

[56] H. Chen, Y. Li, J. L. Rebelatto, B. F. Uchoa-Filho, and B. Vucetic, "Harvest-then-cooperate: Wireless-powered cooperative communications," *IEEE Transactions on Signal Processing*, vol. 63, no. 7, pp. 1700–1711, 2015.

[57] B. Clerckx, R. Zhang, R. Schober, D. W. K. Ng, D. I. Kim, and H. V. Poor, "Fundamentals of wireless information and power transfer: From RF energy harvester models to signal and system designs," *IEEE Journal on Selected Areas in Communications*, vol. 37, no. 1, pp. 4–33, 2018.

[58] Z. Ding, C. Zhong, D. W. K. Ng, M. Peng, H. A. Suraweera, R. Schober, and H. V. Poor, "Application of smart antenna technologies in simultaneous wireless information and power transfer," *IEEE Communications Magazine*, vol. 53, no. 4, pp. 86–93, 2015.

[59] D. W. K. Ng, E. S. Lo, and R. Schober, "Multiobjective resource allocation for secure communication in cognitive radio networks with wireless information and power transfer," *IEEE Transactions on Vehicular Technology*, vol. 65, no. 5, pp. 3166–3184, 2015.

[60] Ng, Derrick Wing Kwan and Lo, Ernest S and Schober, Robert, "Energy-efficient resource allocation in multiuser OFDM systems with wireless information and power transfer," in *2013 IEEE Wireless communications and networking conference (WCNC)*. IEEE, 2013, pp. 3823–3828.

[61] D. W. K. Ng, L. Xiang, and R. Schober, "Multi-objective beamforming for secure communication in systems with wireless information and power transfer," in *2013 IEEE 24th annual international symposium on personal, indoor, and mobile radio communications (PIMRC)*. IEEE, 2013, pp. 7–12.

[62] D. W. K. Ng and R. Schober, "Max-min fair wireless energy transfer for secure multiuser communication systems," in *2014 IEEE Information Theory Workshop (ITW 2014)*. IEEE, 2014, pp. 326–330.

[63] Q. Shi, L. Liu, W. Xu, and R. Zhang, "Joint transmit beamforming and receive power splitting for MISO SWIPT systems," *IEEE Transactions on Wireless Communications*, vol. 13, no. 6, pp. 3269–3280, 2014.

[64] G. Yu, X. Chen, C. Zhong, D. W. Kwan Ng, and Z. Zhang, "Design, analysis, and optimization of a large intelligent reflecting surface-aided b5g cellular internet of things," *IEEE Internet of Things Journal*, vol. 7, no. 9, pp. 8902–8916, 2020.

[65] C. Pan, H. Ren, K. Wang, M. Elkashlan, A. Nallanathan, J. Wang, and L. Hanzo, "Intelligent reflecting surface aided MIMO broadcasting for simultaneous wireless information and power transfer," *IEEE Journal on Selected Areas in Communications*, vol. 38, no. 8, pp. 1719–1734, 2020.

[66] S. Hu, Z. Wei, Y. Cai, C. Liu, D. W. K. Ng, and J. Yuan, "Robust and secure sum-rate maximization for multiuser MISO downlink systems with self-sustainable IRS," *IEEE Transactions on Communications*, vol. 69, no. 10, pp. 7032–7049, 2021.

[67] S. Zargari, A. Khalili, and R. Zhang, "Energy efficiency maximization via joint active and passive beamforming design for multiuser MISO IRS-aided FISWIPT," *IEEE Wireless Communications Letters*, vol. 10, no. 3, pp. 557–561, 2020.

[68] S. Zargari, A. Khalili, Q. Wu, M. R. Mili, and D. W. K. Ng, "Max-min fair energy-efficient beamforming design for intelligent reflecting surface-aided SWIPT systems with non-linear energy harvesting model," *IEEE Transactions on Vehicular Technology*, vol. 70, no. 6, pp. 5848–5864, 2021.

[69] Q. Wu and R. Zhang, "Joint active and passive beamforming optimization for intelligent reflecting surface assisted SWIPT under QoS constraints," *IEEE Journal on Selected Areas in Communications*, vol. 38, no. 8, pp. 1735–1748, 2020.

[70] C. Liu, X. Liu, D. W. K. Ng, and J. Yuan, "Deep residual learning for channel estimation in intelligent reflecting surface-assisted multi-user communications," *IEEE Transactions on Wireless Communications*, vol. 21, no. 2, pp. 898–912, 2021.

[71] J. Xu, L. Liu, and R. Zhang, "Multiuser miso beamforming for simultaneous wireless information and power transfer," *IEEE Transactions on Signal Processing*, vol. 62, no. 18, pp. 4798–4810, 2014.

[72] D. Xu, V. Jamali, X. Yu, D. W. K. Ng, and R. Schober, "Optimal resource allocation design for large irs-assisted SWIPT systems: A scalable optimization framework," *IEEE Transactions on Communications*, vol. 70, no. 2, pp. 1423–1441, 2022.

[73] Z.-Q. Luo, W.-K. Ma, A. M.-C. So, Y. Ye, and S. Zhang, "Semidefinite relaxation of quadratic optimization problems," *IEEE Signal Processing Magazine*, vol. 27, no. 3, pp. 20–34, 2010.

[74] X. Yu, D. Xu, D. W. K. Ng, and R. Schober, "IRS-assisted green communication systems: Provable convergence and robust optimization," *IEEE Transactions on Communications*, vol. 69, no. 9, pp. 6313–6329, 2021.

[75] X. Yu, D. Xu, Y. Sun, D. W. K. Ng, and R. Schober, "Robust and secure wireless communications via intelligent reflecting surfaces," *IEEE Journal on Selected Areas in Communications*, vol. 38, no. 11, pp. 2637–2652, 2020.

[76] S. Boyd, S. P. Boyd, and L. Vandenberghe, *Convex optimization*. Cambridge university press, 2004.

[77] Y. Cai, Z. Wei, R. Li, D. W. K. Ng, and J. Yuan, "Joint trajectory and resource allocation design for energy-efficient secure UAV communication systems," *IEEE Transactions on Communications*, vol. 68, no. 7, pp. 4536–4553, 2020.

[78] T. H. Cormen, C. E. Leiserson, R. L. Rivest, and C. Stein, *Introduction to algorithms*. MIT press, 2022.

[79] Q. Qi, X. Chen, and D. W. K. Ng, "Robust beamforming for NOMA-based cellular massive IoT with SWIPT," *IEEE Transactions on Signal Processing*, vol. 68, pp. 211–224, 2019.

[80] X. Chen, R. Jia, and D. W. K. Ng, "On the design of massive non-orthogonal multiple access with imperfect successive interference cancellation," *IEEE Transactions on Communications*, vol. 67, no. 3, pp. 2539–2551, 2018.

[81] K. B. Petersen, M. S. Pedersen *et al.*, "The matrix cookbook," *Technical University of Denmark*, vol. 7, no. 15, p. 510, 2008.